Never Landing Drone

Autonomous Control for Orographic Soaring of Fixed-Wing UAVs

Master Thesis

T. Suys

Delft University of Technology

TU Delft

Never Landing Drone

Autonomous Control for Orographic Soaring of Fixed-Wing UAVs

by

T. Suys

Master thesis to obtain the degree of Master of Science
at Delft University of Technology,
to be defended publicly on Wednesday May 17, 2023 at 13:00.

Student number:	4464036	
Thesis committee:	Prof. Dr. G. C. H. E. de Croon	TUDelft
	Dr. E. J. J. Smeur	TUDelft
	Dr. B. W. van Oudheusden	TUDelft
	Ir. B.D.W. Remes	TUDelft
	Ir. S. Hwang	TUDelft

Cover Image: Orographic soaring in the dunes, Source: self

TU Delft

Preface

It is with great pleasure that I present this thesis report, which is the culmination of two years of research conducted at Delft University of Technology. My academic journey in Delft began in 2015, and over the course of my studies, I have been fortunate enough to work with some exceptional individuals. I would like to express my sincere gratitude to my supervisors, Guido, Bart, and Sunyou, for their guidance, support, and encouragement throughout this research. Additionally, the MAVLab team's support and collaboration were essential to this project's success. I would like to take this opportunity to thank my family, friends, and girlfriend for their encouragement and support throughout my studies, without which this accomplishment would not have been possible.

The research presented in this report proposes a novel approach to extending the endurance of fixed-wing UAVs through autonomous soaring in an orographic wind field. I am immensely proud that this research has been accepted for inclusion in the conference proceedings of the IEEE International Conference on Robotics and Automation (ICRA), which I consider to be the highlight of my academic career.

Thank you for your curiosity in reading my work, and I hope that this report inspires further research and innovation in the field.

T. Suys
Delft, April 2023

Contents

Abstract

Prolonging the endurance of fixed-wing UAVs is crucial for achieving complex missions, yet their limited battery life poses a significant challenge. In response, this research proposes a novel approach to extend the endurance of fixed-wing UAVs by enabling autonomous soaring in an orographic wind field. The goal of our research is to develop a controller that can identify feasible soaring regions and autonomously maintain position control without using any throttle. Soaring flight is desirable as it results in a low energy cost with zero throttle usage. However, without throttle usage, the longitudinal motion of the UAV is an under-actuated system, presenting control challenges. The concept of a target gradient line (TGL) is introduced as part of the control algorithm that addresses these challenges and autonomously finds the equilibrium soaring position where sink rate and updraft are in equilibrium. Experimental tests showed promising results, demonstrating the controller's effectiveness in maintaining autonomous soaring flight in a non-static wind field. We also demonstrate a single degree of control freedom in the soaring position through manipulation of the TGL.

Nomenclature

Abbreviations

Abbreviation	Definition
CFD	Computational Fluid Dynamics
CG	Center of Gravity
GNSS	Global Navigation Satellite Systems
MAV	Micro Air Vehicle
OJF	Open Jet Facility
TECS	Total Energy Control System
TGL	Target Gradient Line
TU Delft	Delft University of Technology
RMIT	Royal Melbourne Institute of Technology
RSSI	Received Signal Strength Indicator
RTK	Real Time Kinematics
UAV	Unmanned Aerial Vehicle
UWB	Ultra Wide Band
ZEUC	Zero Excess Updraft Contour

Symbols

Symbol	Definition	Unit
C_L	Lift coefficient	$[-]$
D	Drag force	$[N]$
E_k	Kinetic energy	$[J]$
E_p	Potential energy	$[J]$
g	Gravitational acceleration (9.80665)	$[m/s^2]$
h	Height	$[m]$
L	Lift force	$[N]$
m	Mass	$[kg]$
r	Polar distance	$[m]$
s	Time	$[s]$
S	Wing surface area	$[m^2]$
T	Thrust force	$[N]$
v_a	Air speed	$[m/s]$
V	Velocity	$[m/s]$
w_x	Horizontal wind component	$[m/s]$
w_z	Vertical wind component	$[m/s]$
$\dot{(x)}_i$	Horizontal velocity component (inertial frame)	$[m/s]$
$\dot{(z)}_i$	Vertical velocity component (inertial frame)	$[m/s]$
α	Angle of attack	$[rad]$
δ_a	Aileron deflection	$[rad]$
δ_e	Elevator deflection	$[rad]$
δ_r	Rudder deflection	$[rad]$
δ_t	Thrust	$[rad]$
ρ	Air density	$[kg/m^3]$

Symbol	Definition	Unit
γ	Flight path angle	[rad]
θ	Polar angle	[rad]
θ	Pitch angle	[rad]

List of Figures

List of Tables

1 Introduction

1.1. Motivation

Unmanned Aerial Vehicles (UAVs) are increasingly more commonplace. A shift in public perspective and recent technological advances are contributing factors to a wider adoption of UAVs. Next to recreational use and amateur film making, UAVs also play an important role in the industry. Maintenance, inspection, mapping, surveying and agriculture are among the top use cases for drones globally. The drone market is a multi billion dollar industry, consistently growing at a seemingly unstoppable annual growth rate of over 14% [1].

The endurance of these UAVs is a major constraint for most missions. Several methods have been proposed and implemented to increase flight time. A notable distinction is that fixed-wing UAVs can benefit from a lower energy consumption than their hovering counterparts. Large UAVs can explore alternative energy sources such as combustible fuels or hydrogen generators. Smaller UAVs have also benefited from the miniaturization of avionics and improvements in battery technology. In spite of these efforts, the full potential of many UAV applications remains limited by a reduced flight time.

Therefore, researching other techniques that can positively impact the effective endurance of these UAVs is essential. An interesting method that has shown great potential lies in exploiting updrafts to stay airborne nearly indefinitely. Albatrosses have perfected the technique of soaring, enabling very efficient flight where they stay airborne without flapping their wings. The ability to fly at no mechanical energy cost allows these birds to embark journeys in excess of 20000km, staying airborne for multiple days at a time. This performance is orders of magnitude beyond the capabilities of current UAVs of a comparable size. A testimony of the huge potential that lies in soaring as a method to extend endurance.

1.2. Research question

In order to effectively conduct this thesis project it is important to formulate the research question. This is done through the means of a main research question and sub questions that the author seeks to answer during the project. The main research question has been formulated as follows:

Primary Research Question:

Is it feasible for a fixed-wing UAV to achieve a near unlimited endurance through autonomous orographic soaring?

It is useful to break down the components of the research question so their meaning is unambiguous.

- **UAV** — An unmanned aerial vehicle capable of autonomous flight. This projects considers vehicles in the size range of a Micro Air Vehicle (MAV) until hobby grade RC planes with a wingspan smaller than 2 meter.
- **fixed wing** — Multirotors and flapping wing variations of UAVs are excluded in this study.
- **near unlimited endurance** — Available on board power to run a propulsion system is no longer the main constraint in the UAVs endurance. Of course, the power requirements of other subsystems and components would still drain the battery, but at much lower rate.
- **autonomous** — The ability of the UAV to stay airborne without continuous intervention of a human operator.
- **orographic soaring** — The subset of static soaring where updraft is caused by the rising air on the windward side of a slope. More context is given in chapter 2.

Also notice how this is formulated as a polar question that could essentially be answered by yes or no. Therefore it useful to add sub questions to further define the objective and scope of this project.

Sub question 1:
What degree of position control is possible while soaring?

UAVs in a classical fixed-wing configuration have full control actuation around their principal axis and full throttle authority for their position control. It can be foreseen that in the case of soaring flight the control authority is dependent on the wind field. It is interesting to study what degree of control remains possible and to what extend soaring capabilities are affected. Furthermore, minimizing or fully negating throttle usage further reduces control freedom, it is worthwhile to study if position control is possible in propulsion-less soaring flight.

Sub question 2:
How is the control system affected when the windfield changes?

Multiple variables can be manipulated in a soaring condition. The environmental conditions can change, but also the shape of the object that is deflecting the wind. It is worthwhile to study how changes in the wind velocity affect the windfield and soaring capability of the controller. Usually the wind deflection is by static obstacles such as hills or buildings. It is interesting to consider a changing wind deflection angle over an object. It is also interesting to consider the case of a moving obstacle. An example of this is the updraft around a moving ship in open sea.

1.3. Research objectives

This research is done in collaboration with the MAVLab. The MAVLab prides itself with extensive real world experimental tests and results to back up research findings. The research objectives presented below focus on the more practical accomplishments that this research seeks to attain.

Primary research objective:

Demonstrate autonomous orographic soaring of a UAV in a real world test setup.

The primary objective can be subdivided in multiple sub goals. This structures the research development and defines a sequence of goals at an increasing level of complexity.

Sub goal 1:
Model an orographic windfield and define feasible soaring regions.

A crucial first step in the research is modelling the orographic wind field. This is needed to gain insight in how and where the updraft is created and which factors affect the windfield. Furthermore it is required to find the regions in the windfield where the updraft is sufficient to sustain soaring flight. Having a model will aid in gaining insight in the flight dynamics of the UAV while in soaring condition. This is necessary to effectively develop a controller that can realize autonomous soaring flight.

Sub goal 2:
Develop an autonomous controller capable of soaring flight.

With a model, different control strategies can be tested at a high pace and low cost. Different strategies can be compared in performance before real world testing commences.

Sub goal 3:
Develop an initial test UAV and experimental test setup

A fixed wing UAV needs to be constructed with the necessary hardware on board capable of autonomous control. Furthermore a test environment needs to constructed where an orographic updraft can be created. Ideally, the test environment is controlled and variables can be individually adjusted.

Sub goal 4:
Demonstrate effectiveness in a non-static wind field and position control.

When steady soaring flight is demonstrated, the controller should be subjected to changing environmental conditions. This can be done in a controlled manner in an indoor test facility or outdoors, leveraging the atmospheric variations in wind. Furthermore, it is interesting to test the controller when manipulating the deflection angle of the updraft. Finally, capability for position control of the UAV can be tested and demonstrated.

Sub goal 5:
Experimentally determine the controller limitations.

The final goal in the research is to determine the controller's limitations. As many external variables as is practical should be adjusted until failure. This helps to define the limitations of tested controller and will aid in further development and research.

1.4. Structure of this work

Following the introduction which introduced the motivation and research question, this report is divided in 4 parts.

Part I is the scientific paper on this research. This paper contains the main contributions of this thesis and can be read as a standalone document. This paper has been accepted for presentation at the 2023 IEEE International Conference on Robotics and Automation (ICRA), May 29 - June 2, 2023, ExCeL London, UK, and for inclusion in the conference proceedings.

Part II consists of the literature study that was conducted for this research. Directly relevant literature on autonomous orographic soaring itself is limited. Therefore, four different research focus areas have been defined to explore the developments in this field. This part will discuss the fundamentals of soaring in chapter 2. An analysis and study of orographic wind fields is presented in chapter 3. In chapter 4 the constraints on control freedom while soaring are explored. Furthermore, his chapter discusses the relevant literature related to the control aspects of autonomous orographic soaring. Finally, chapter 5 provides an overview of various relevant positioning systems and attitude determination systems.

Part III contains additional findings that were not included in the paper as well as more info on the performed flight tests. chapter 6 highlights the results of an outdoor manual dune soaring test that was performed. In chapter 7, additional context is given on the indoor flight test that was performed in the Open Jet Facility.

Finally, is a synthesis of this work. This part contains a conclusion in chapter 8. This report ends with recommendations for future work in chapter 9. Future research directions and alternative approaches are discussed.

I

Scientific Paper

Autonomous Control for Orographic Soaring of Fixed-Wing UAVs

Tom Suys[1], Sunyou Hwang[1], Guido C.H.E. de Croon[1], and Bart D.W. Remes[1]

***Abstract*— We present a novel controller for fixed-wing UAVs that enables autonomous soaring in an orographic wind field, extending flight endurance. Our method identifies soaring regions and addresses position control challenges by introducing a target gradient line (TGL) on which the UAV achieves an equilibrium soaring position, where sink rate and updraft are balanced. Experimental testing validates the controller's effectiveness in maintaining autonomous soaring flight without using any thrust in a non-static wind field. We also demonstrate a single degree of control freedom in a soaring position through manipulation of the TGL.**

***Index Terms*— wind hovering, orographic soaring, autonomous control, UAV**

I. INTRODUCTION

UAVs have benefited from advancements in battery technology and miniaturization of avionics, which resulted in an increase in their endurance and range. However, the full potential of UAV applications remains limited by reduced flight time. Therefore, it is useful to research other techniques that can positively impact the effective endurance of these UAVs. An interesting technique that has shown great potential is exploiting updrafts to stay airborne nearly indefinitely. Albatrosses have perfected this technique of soaring [1], [2], allowing them to fly without mechanical energy cost and embark on journeys exceeding 20,000 km, staying airborne for multiple days at a time [3], [4].

All soaring techniques aim to extract sufficient energy to stay airborne without losing altitude. Dynamic soaring is when energy is extracted due to a gradient in the horizontal wind velocity [5], while static soaring relies on a vertical, upward wind component. Static soaring includes two types: thermal soaring, which is created by a rising column of air, and orographic soaring, which is created by the upwards deflection of the wind stream. This research focuses exclusively on orographic soaring.

Prior research has explored the potential of exploiting orographic updrafts [6]–[11]. White et al. utilized simulations and measurement data to evaluate the feasibility of soaring in the updraft generated by tall buildings. However, flight demonstrations were not conducted in these studies. While some studies have demonstrated orographic soaring [12], [13], they require a priori knowledge of the wind field and manual control of a human pilot to steer the UAV to an initial soaring position. Above studies considered a static wind field and predetermined path of the UAV.

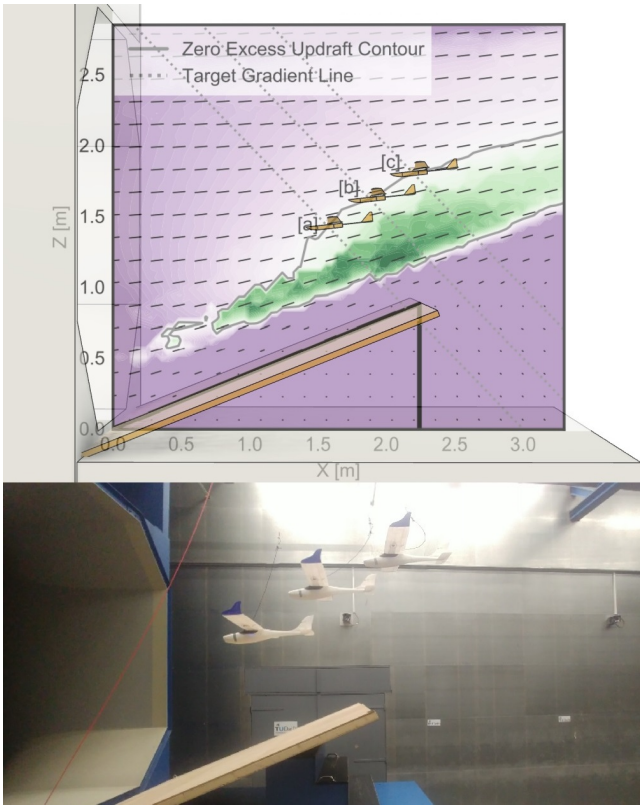

Fig. 1. Autonomous soaring and position control of an UAV. The model shows the predicted excess updraft in the orographic wind field of the test setup. By precisely maintaining position control along an operator-specified target gradient line, the UAV successfully achieves autonomous soaring flight at the intersection with zero-excess updraft. The observed flight data, presented as three stacked stills in the image, correspond to the predicted soaring locations for three distinct target gradient lines specified in the test.

In contrast, with this paper we propose a novel orographic soaring method with a single degree of control freedom, which can adapt to a non-static wind field, and does not require any throttle usage. Our method utilizes information derived from the approximate location of the updraft core but does not require complete prior knowledge of the wind field. We demonstrate fully autonomous soaring flight, and a single degree of position control of a UAV without propeller in a non-static wind field in a real-world test. We derive the kinematics involved with orographic soaring in section II. Its distinct control freedom is outlined in section III. Potential flow is used to estimate a soaring wind field in section IV. In section V, a control strategy is proposed to maintain autonomous soaring flight. The experimental test setup and test results are discussed in section VI and section VII.

[1]All authors are with the MAVLab, Department of Control and Operations, Faculty of Aerospace Engineering, Delft University of Technology, 2629HS Delft, the Netherlands mail@tomsuys.com, S.Hwang-1@tudelft.nl, G.C.H.E.deCroon@tudelft.nl, B.D.W.Remes@tudelft.nl

A supplementary video of the flight tests is available at: https://youtu.be/b_YLoinHepo

II. OROGRAPHIC SOARING

The kinematics involved with orographic soaring can be modeled using a point mass model, as illustrated by Langelaan [14]. In this model, we define the vehicle mass (m), angle of attack (α), thrust (T), drag (D), and lift force (L) as key parameters.

First, considering the forces parallel and perpendicular to the flight path, we obtain two equations:

$$mg\cos(\gamma) = L + T\sin(\alpha) \tag{1}$$

$$mg\sin(\gamma) = D - T\cos(\alpha) \tag{2}$$

Here, flight path angle γ is assumed small and a small angle approximation is used. Next, we obtain an equation that relates lift force to other parameters:

$$mg = L = \frac{1}{2}\rho v_a^2 S C_L \tag{3}$$

Using this equation, we can calculate the lift coefficient (C_L) in terms of other parameters:

$$C_L = \frac{2mg}{\rho v_a^2 S} \tag{4}$$

Additionally, we can derive a second-order approximation for the drag force (D):

$$D = \frac{1}{2}\rho v_a^2 S(a_0 + a_1 C_L + a_2 C_L^2) \tag{5}$$

Substituting this approximation into Equation 2, we can calculate the flight path angle for a given speed and thrust:

$$mg\gamma = \frac{1}{2}\rho v_a^2(a_0 + a_1 C_L + a_2 C_L^2) - T \tag{6}$$

Finally, we can describe the aircraft kinematics in terms of airspeed, flight path angle, and wind speed. We define the horizontal ($\dot{x}_i$) and vertical ($\dot{z}_i$) velocity components in the inertial frame and model the wind speed as a polynomial function of position in the inertial frame ($w = f(x_i, z_i)$):

$$\dot{x}_i = v_a\cos(\gamma) + w_x \tag{7}$$

$$\dot{z}_i = v_a sin(\gamma) + w_z \tag{8}$$

III. SOARING CONTROL FREEDOM

The ailerons, elevator, and rudder have a primary control effect on roll, pitch, and yaw respectively. Flight control in powered flight is further augmented by a throttle setpoint, which relates to the thrust reaction force. In the 6 degree of freedom (DOF) equations of motion, the aileron, elevator, rudder deflection, and thrust are the four main actuator control inputs. In this research it is useful to isolate the lateral and longitudinal motion.

Longitudinal motion:

$$\begin{aligned} x &= [\Delta u\ \ \Delta w\ \ \Delta q\ \ \Delta x\ \ \Delta z\ \ \Delta\theta]^T \\ u &= [\Delta\delta E\ \ \Delta\delta T]^T \end{aligned} \tag{9}$$

Lateral motion:

$$\begin{aligned} x &= [\Delta v\ \ \Delta p\ \ \Delta r\ \ \Delta y\ \ \Delta\phi\ \ \Delta\psi]^T \\ u &= [\Delta\delta E\ \ \Delta\delta T]^T \end{aligned} \tag{10}$$

For lateral motion, the dynamics during soaring remain the same. Therefore, the continuation of this report will focus solely on the longitudinal motion. As can be seen in Equation 9, in powered fixed-wing flight, elevator deflection and throttle setpoint are actuator inputs to the system. There are 6 state variables; position in the vertical plane, velocity in the vertical plane, pitch angle, and pitch rate.

Consider the available control freedom in the longitudinal motion of powered fixed-wing flight. Granted that the control objectives adhere to the nonholonomic constraints of the system, one is able to satisfy 2 of the 3 DOF. Fundamentally, this allows longitudinal control systems, such as a total energy control system to function [15]. Throttle and elevator control input are used to obtain a desired position and velocity in the vertical plane, resulting in pitch angle and pitch rate as dependent, uncontrollable variables.

The design of a soaring control strategy aims to eliminate throttle usage, leaving elevator deflection as the sole control actuator in the longitudinal motion. As a result, in this under-constrained system, traditional position control is not a viable option, and a novel approach is required.

IV. WIND FIELD ANALYSIS

In the development of an orographic soaring control strategy, it is useful to consider methods to analyse and simulate a viable soaring wind field. A simplified potential flow model can be used for this, which estimates the wind field over an idealized hill with a semi-circular cross-section. [16], [17].

Potential flow around a cylinder can be obtained by considering a uniform stream of velocity (U) and a doublet at the center of the cylinder such that the stagnation point precisely matches the boundary of the cylinder. The solution is most easily obtained in polar coordinates:

$$\Phi(r,\theta) = Ur(1 - \frac{R^2}{r^2}cos(\theta)) \tag{11}$$

The velocity in polar coordinates is then:

$$V_r = \frac{\delta\Phi}{\delta r} = U(1 - \frac{R^2}{r^2}cos(\theta)) \tag{12}$$

$$V_\theta = \frac{1}{r}\frac{\delta\Phi}{\delta\theta} = -U(1 + \frac{R^2}{r^2}sin(\theta)) \tag{13}$$

This can be related to Cartesian coordinates by substituting $x = rcos(\theta)$ and $y = rsin(\theta)$.

The wind field is illustrated in Figure 2, which shows the upper windward quadrant as an orographic wind field. Of particular interest in the wind field is the vertical wind component, which should match the sink rate of the UAV to sustain soaring flight.

Therefore, for soaring flight it is useful to consider the glide polar of an airframe, as it precisely describes the relationship between airspeed and sink rate. At the maximum endurance speed (V_{ME}) a particular airframe will experience the lowest rate of sink. At lower velocities the airfoil will enter its stall regime and sink rate will increase. To maintain higher velocities than V_{ME} during unpowered flight, the aircraft has to assume a nose-down attitude and the sink rate

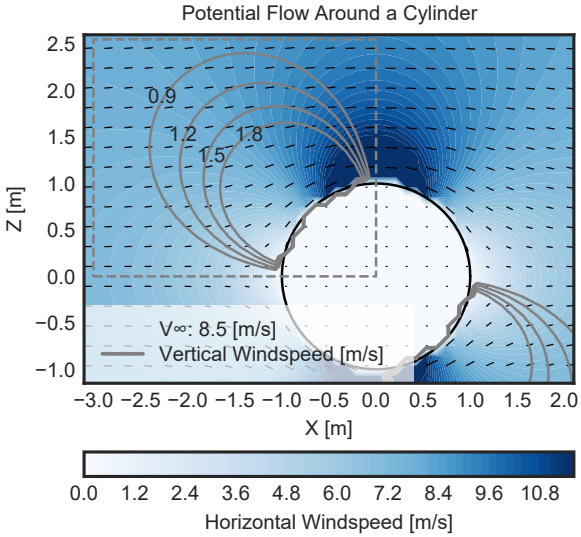

Fig. 2. Wind velocity components around a cylinder obtained with potential flow theory. The upper windward quadrant is an orographic wind field.

will increase as well. An arbitrary quadratic function that follows the characteristics of a glide polar is chosen to study its effect in an orographic soaring wind field.

As introduced by Fisher et al. [12], we can determine the feasible soaring region. At every point in the wind field, the local vertical updraft component is compared to the expected sink rate at the local horizontal wind velocity according to the glide polar. In this research we introduce the zero excess updraft contour (ZEUC); the line in the windfield where the expected local updraft equates the sink rate. The inner region defined by the ZEUC has an excess in updraft and the outer region has a lack of sufficient updraft. The process is illustrated in Figure 3. The aircraft is able to maintain its soaring position at every point on this contour. Three different soaring positions and their respective state on the glide polar are mapped. At $[a]$ and $[c]$, the aircraft will experience the same sink rate of $1.7m/s$ at a different horizontal velocity wind component, whereas in $[b]$ the aircraft requires the least updraft to maintain its soaring position.

V. AUTONOMOUS CONTROL STRATEGY

As concluded in section III, the longitudinal motion of a soaring UAV is an under-actuated system. The feasible region where the UAV can soar efficiently in the vertical plane is limited to a specific contour line called zero excess updraft contour (ZEUC), as outlined in section IV. However, the location of this contour line cannot be determined without prior knowledge of the wind field, which complicates the use of a position controller. To address this issue, we introduce a target gradient line (TGL) as a novel approach to control the UAV's position.

The TGL represents a path in the wind field along which there is a gradient in the available updraft. The TGL is chosen thoughtfully to originate at a point in the wind field where there exists excess updraft and extends upwards to a region

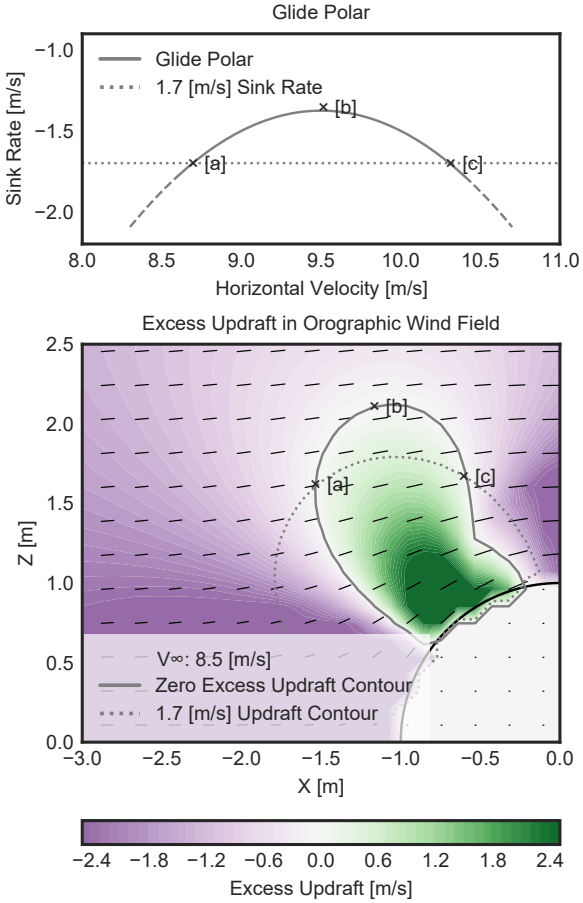

Fig. 3. The glide polar defines the relation of the sink rate and horizontal velocity. Mapping of this glide polar on the orographic wind field yields the zero excess updraft contour. Three different soaring positions and their respective state on the glide polar are mapped.

of lack in updraft. The UAV utilizes its single degree of longitudinal control to maintain position on the TGL but is free to move along it. As a result, the UAV naturally settles in an equilibrium at the intersection of the TGL and ZEUC. This approach simplifies the control strategy, making it easier to implement and more robust to variations in the wind field.

The natural equilibrium soaring location of the UAV can be influenced by several factors. Firstly, the operator can manipulate the UAV's position along the ZEUC by rotating or translating the TGL in the vertical plane, thereby realizing a single degree of control freedom. Secondly, during flight, small changes in the wind field are expected, which can result in a changing position of the ZEUC. By maintaining position on the TGL, The UAV will naturally move along the TGL to a new equilibrium point, which will be at the intersection with the ZEUC.

The controller to maintain position on the TGL is implemented as a closed-loop pitch controller. The perpendicular distance of the UAV to the TGL, (e_ρ), is formulated as an error input for the controller. By convention, e_ρ is positive when the UAV is upstream of the TGL and negative when the UAV is downstream, defined in Equation 14.

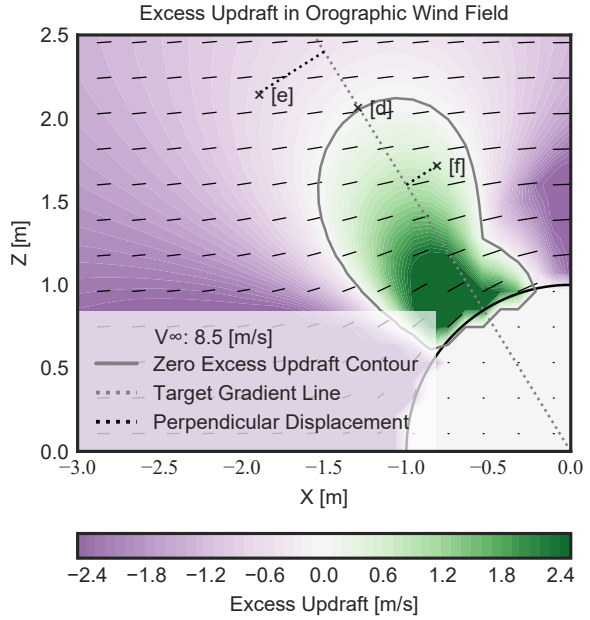

Fig. 4. The autonomous control strategy considers a target gradient line intersecting the zero excess updraft contour. The controller response is proportional to the perpendicular displacement to the TGL.

$$e_\rho = s * \frac{|Ax_1 + Bz_1 + C|}{A^2 + B^2} \quad \text{with} \quad \begin{matrix} s = \quad 1 \text{ IF upstream} \\ s = -1 \text{ IF downstream} \end{matrix} \tag{14}$$

With $TGL: Ax + Bz + C = 0$ and UAV position $P: (x_1, z_1)$. The implementation is the test setup is analogous, where instead the TGL is extruded along y, and the perpendicular distance to said target plane is considered.

The pitch setpoint is then obtained as follows:

$$\theta_{sp} = \theta_0 + e_\rho + k_i \int e_\rho dt + k_d \frac{de_\rho}{dt} \tag{15}$$

θ_0 is the trimmed pitch angle at the expected flight velocity. Stable soaring flight can be achieved by tuning the proportional (k_p) and derivative (k_d) gains. The use of an integral gain (k_i) is recommended to minimise steady-state error and realise full convergence to the TGL. The elevator setpoint (e_{sp}) is controlled with a closed-loop controller, taking as input the pitch error (θ_e).

$$e_{sp} = k_p \theta_e + k_i \int \theta_e dt + k_d \frac{d\theta_e}{dt} \tag{16}$$

The TGL can be thoughtfully chosen to best deal with disturbances to the equilibrium. Namely, the total energy state of the vehicle in immediate proximity to the TGL should be considered. For instance, a horizontal TGL would often be a poor choice. A vehicle that finds itself below the TGL might lack the potential energy as well as higher updraft regions to regain altitude towards its TGL. Furthermore, a TGL is best chosen roughly perpendicular to the ZEUC. This way, minimal displacement along the TGL is required to accommodate changes in the wind field. It is important to note that this control strategy does not require a priori knowledge of the wind field. However, a general estimate of the shape of the wind field, such as knowledge of the location of the updraft core, is desired to effectively choose a TGL.

VI. EXPERIMENTAL TEST SETUP

We conducted a full-scale test campaign in the open jet facility at Delft University of Technology. The facility has an outlet cross-section of $2.85m$ and can generate wind velocities up to $35m/s$. An updraft was created by placing a board at various angles in the airflow. We used this geometry to create a CFD model to estimate wind velocity components in the test section at various wind velocities and slope positions. [18]. The geometry is highlighted in Figure 1 and the velocity components are shown in Figure 5.

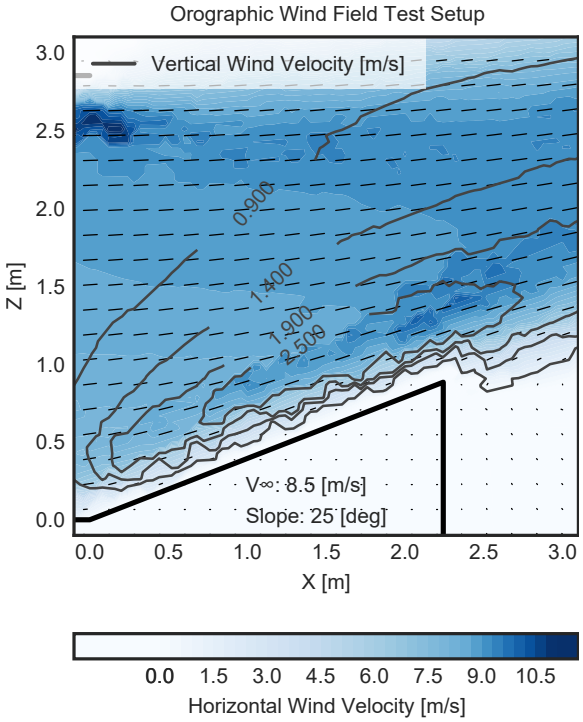

Fig. 5. Wind velocity components of the orographic wind field in the experimental test setup, obtained by CFD.

The test UAV was a modified Eclipson Model C [19] 3D-printed model aircraft running Paparazzi autopilot [20]. The aircraft had three degrees of actuation with aileron, rudder, and elevator but no propeller. We determined the aircraft's glide polar by third-order polynomial regression of gliding flight data at discretely different pitch attitudes. This glide polar is shown in Figure 7. We used an Optitrack system [21], mounted in the test facility, to receive the aircraft's positioning data, which was also logged to evaluate the controller's performance. An image of the test setup and its components is shown in Figure 6.

To ensure lateral stability and heading during testing, we implemented two lateral closed-loop control systems. The roll controller affects the ailerons and keeps the aircraft level, while the yaw controller affects the rudder and maintains the heading towards a virtual waypoint located $5m$ upwind from

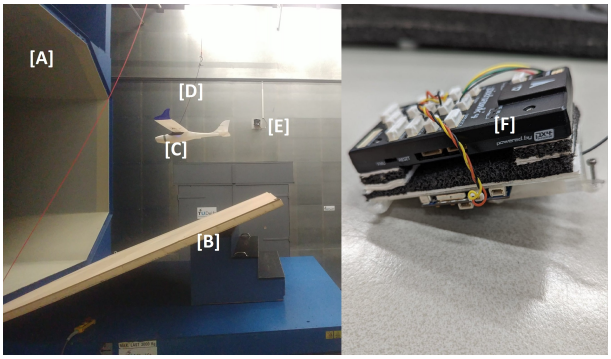

Fig. 6. Test setup and data collection. [A] Open Jet Facility wind tunnel, [B] Adjustable slope, [C] UAV (without propeller mounted), [D] Safety tether, [E] Optitrack system camera, [F] Pixhawk 4 running Paparazzi autopilot

the wind tunnel settling chamber, achieving centering within the wind tunnel cross-section. The yaw error is defined as $e_\psi = \tan(y/R) - \psi$, where y is the displacement from the vertical center plane in the wind tunnel and R is the distance to the virtual upwind waypoint.

Both actuator setpoints are obtained through a closed-loop control system with proportional (k_p), integral (k_i), and derivative (k_d) gains, as shown in Equations 17 and 18. The novel soaring controller, presented in section V, affects the elevator.

$$a_{sp} = k_p e_\phi + k_i \int e_\phi dt + k_d \frac{de_\phi}{dt} \tag{17}$$

$$r_{sp} = k_p e_\psi + k_d \frac{de_\psi}{dt} \tag{18}$$

Our primary goal was to validate the novel soaring controller and investigate the effect of changing the slope, wind speed, and placement of the TGL.

VII. TEST RESULTS AND DISCUSSION

By combining the velocity components in the wind field from CFD simulations and the glide polar, the (ZEUC) can be generated, as shown in Figure 7. It should be noted that the required updraft along the ZEUC is not a constant amount. It is a function of the local horizontal wind velocity component and the glide polar.

In Figure 7, consider a test with the leftmost static TGL at position $[a]$. After manual tuning of the controller gains, it is observed from the flight path that the controller is able to successfully maintain position with minimal oscillations. Note that the TGL was chosen to be roughly perpendicular to the ZEUC. Defining a TGL less perpendicular to the ZEUC negatively affected the controller performance with larger oscillations and drift from the TGL.

As we translate the TGL to positions $[b]$ and $[c]$, the settled equilibrium of the aircraft also moves along with the TGL. Each equilibrium point corresponds to a different part of the aircraft's glide polar. Notably, the flight path positions recorded during the test closely coincide with the intersection of the TGL and ZEUC. This confirms the effectiveness of

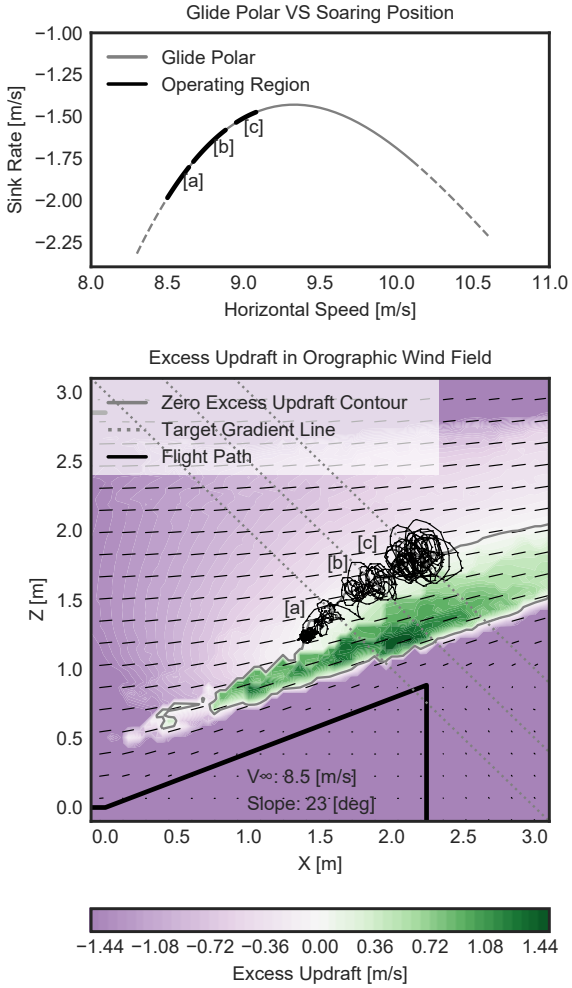

Fig. 7. Mapping of the Eclipson Model C glide polar on the orographic wind field of the experimental test setup, yielding the expected zero excess updraft contour. Three different TGL positions are tested and the corresponding flight path is plotted. Note that the flight path corresponds well with the expected soaring locations.

the controller in maintaining position on the chosen TGL and the accuracy of the estimated wind field and glide polar. Additionally, moving the TGL proves to be an effective method for achieving a single degree of position control freedom with this soaring controller. Larger oscillations were observed downstream as a result of overshoot due to the increased elevator effectiveness at higher airspeed.

In Figure 8, we investigated the effect of changing the slope in the test setup on the resultant ZEUC. We increased the slope from 23 to 25 degrees and observed that the contour shifted upwards. To study the controller's adaptability to changes in the wind field, we repeated the testing with incremental translation of the TGL at this higher slope. Our results show that the controller was able to adapt to changes in the wind field while maintaining the same level of control freedom.

Next, we examined the effect of changes in wind speed on the UAV's performance. We incrementally increased the wind speed from 8.5 to 9.5 m/s while maintaining the same TGL. Throughout this range, the UAV was able to success-

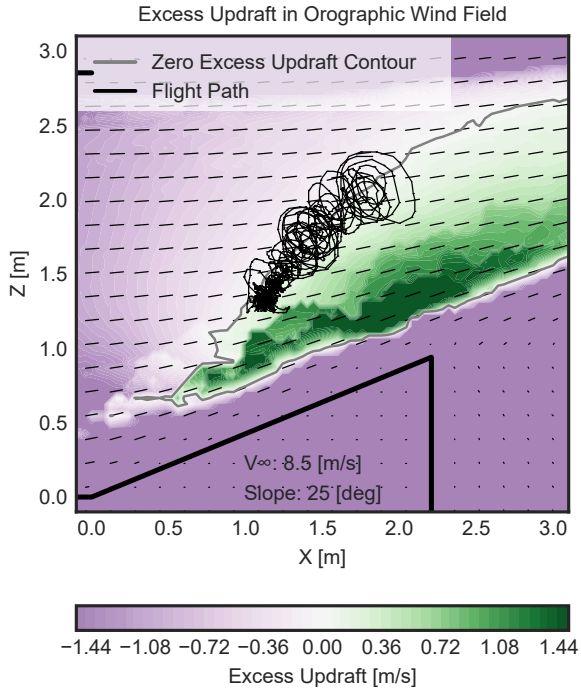

Fig. 8. Effect of changing the slope from 23*deg* to 25*deg*. The zero excess updraft contour (ZEUC) is now located noticeably higher. The flight path is plotted over a translating TGL. From the flight track we observe that the soaring location corresponds with the newly obtained ZEUC.

fully maintain soaring flight, and we did not observe any significant changes in its hovering position. This unexpected result can be explained by considering the immediate effect of changes in horizontal wind velocity on the updraft and sink rate. We assumed that the vertical updraft component would scale proportionally to the horizontal wind. Therefore, a change in wind velocity would not change the shape of the wind field, but it would only scale the magnitude of all local wind vectors.

Consider Figure 9, which presents three scenarios where the updraft and sink rate are initially balanced.

- In scenario [a], the airfoil is in the stall regime and a change in wind velocity has a significant impact on the updraft and sink rate. An increase in wind velocity leads to an increase in the updraft component and a decrease in the sink rate, resulting in a net upward movement. Conversely, a decrease in wind velocity causes a net downward movement.
- In scenario [c], a change in wind velocity has a greater impact on the sink rate than the updraft, leading to a net downward movement with an increase in wind velocity and a net upward movement with a decrease in wind velocity.
- Finally, when the aircraft is operating near its optimal glide speed in the vicinity of [b], changes in wind velocity cause both the updraft and sink rate to change at a comparable rate, resulting in minimal movement. This scenario was observed during the experimental test and helps explain that limited movement was observed.

A change in wind velocity alters the shape and position of the ZEUC accordingly. The reaction force resulting from an imbalance between updraft and sink rate allows the aircraft to settle on the newly obtained ZEUC.

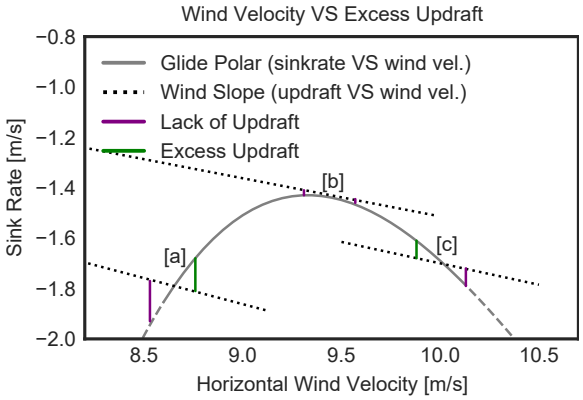

Fig. 9. Comparison of the immediate change in sink rate and updraft as a result of changing the horizontal wind velocity at different segments on the glide slope. Changes in wind velocity affect the generated updraft in the wind field and effective sink rate of the aircraft differently.

VIII. CONCLUSIONS

The objective of this research was to demonstrate the feasibility of autonomous orographic soaring for fixed-wing UAVs. We identified the feasible soaring region, which can be represented by a single line known as the zero excess updraft contour (ZEUC).

As the longitudinal motion of a soaring UAV is an under-actuated system, we introduced the concept of a target gradient line (TGL) to provide a single degree of control freedom. We then presented an autonomous controller that enables position keeping at the intersection of the TGL and ZEUC. We validated the controller in an experimental test setup, and the results showed that it effectively maintained position on the chosen TGL without using any thrust as the UAV had no propeller. Furthermore, the position of the logged flight segments closely aligned with the expected ZEUC, which was derived from the estimated wind field and glide polar.

We demonstrated that adjusting the TGL is an effective way to realize a single degree of control freedom in the system. Finally, we showed that the controller is robust to changes in the wind field, such as alterations in slope or changes in the free-stream velocity of the wind tunnel.

The performed tests in this research were limited by the cross-section of the wind tunnel. To enable a larger orographic wind field and more diverse wind conditions, additional testing in an outdoor environment is recommended. Furthermore, this would enable testing in a wider envelope of the UAV's glide polar. When soaring in a broad airspeed range, it is recommended to adjust the gains for changes in elevator effectiveness. Finally, it can be challenging to set a favorable TGL without a priori knowledge of the wind field. Further research on obtaining an initial soaring position is suggested.

REFERENCES

[1] L. Rayleigh, "The soaring of birds," *Nature*, vol. 27, no. 701, pp. 534–535, 1883.

[2] J. Rayleigh, "The sailing flight of the albatross," *Nature*, vol. 40, no. 1019, p. 34, 1889.

[3] H. Weimerskirch, K. Delord, A. Guitteaud, R. A. Phillips, and P. Pinet, "Extreme variation in migration strategies between and within wandering albatross populations during their sabbatical year and their fitness consequences," *Scientific reports*, vol. 5, no. 1, pp. 1–7, 2015.

[4] G. Sachs, J. Traugott, A. P. Nesterova, G. Dell'Omo, F. Kümmeth, W. Heidrich, A. L. Vyssotski, and F. Bonadonna, "Flying at no mechanical energy cost: disclosing the secret of wandering albatrosses," 2012.

[5] Y. J. Zhao, "Optimal patterns of glider dynamic soaring," *Optimal control applications and methods*, vol. 25, no. 2, pp. 67–89, 2004.

[6] C. White, E. W. Lim, S. Watkins, A. Mohamed, and M. Thompson, "A feasibility study of micro air vehicles soaring tall buildings," *Journal of Wind Engineering and Industrial Aerodynamics*, vol. 103, pp. 41–49, 2012.

[7] C. White, S. Watkins, E. W. Lim, and K. Massey, "The soaring potential of a micro air vehicle in an urban environment," *International Journal of Micro Air Vehicles*, vol. 4, no. 1, 2012.

[8] A. Mohamed, R. Carrese, D. Fletcher, and S. Watkins, "Scale-resolving simulation to predict the updraught regions over buildings for mav orographic lift soaring," *Journal of Wind Engineering and Industrial Aerodynamics*, vol. 140, pp. 34–48, 2015.

[9] A. Mohamed, M. Abdulrahim, S. Watkins, and R. Clothier, "Development and flight testing of a turbulence mitigation system for micro air vehicles," *Journal of Field Robotics*, vol. 33, no. 5, 2016.

[10] A. Guerra-Langan, S. Araujo-Estrada, and S. Windsor, "Unmanned aerial vehicle control costs mirror bird behaviour when soaring close to buildings," *International Journal of Micro Air Vehicles*, vol. 12, p. 1756829320941005, 2020.

[11] J. W. Langelaan, N. Alley, and J. Neidhoefer, "Wind field estimation for small unmanned aerial vehicles," *Journal of Guidance, Control, and Dynamics*, vol. 34, no. 4, 2011.

[12] A. Fisher, M. Marino, R. Clothier, S. Watkins, L. Peters, and J. L. Palmer, "Emulating avian orographic soaring with a small autonomous glider," *Bioinspiration & biomimetics*, vol. 11, no. 1, p. 016002, 2015.

[13] C. P. de Jong, B. D. Remes, S. Hwang, and C. De Wagter, "Never landing drone: Autonomous soaring of a unmanned aerial vehicle in front of a moving obstacle," *International Journal of Micro Air Vehicles*, vol. 13, p. 17568293211060500, 2021.

[14] J. Langelaan, "Long distance/duration trajectory optimization for small uavs," in *AIAA guidance, navigation and control conference and exhibit*, 2007, p. 6737.

[15] A. A. Lambregts, "TECS generalized airplane control system design – an update," in *Advances in Aerospace Guidance, Navigation and Control*. Springer Berlin Heidelberg, 2013, pp. 503–534.

[16] J. D. Anderson, "Fundamentals of aerodynamics," *McGraw*, 2009.

[17] M. Gossye, S. Hwang, and B. Remes, "Developing a modular tool to simulate regeneration power potential using orographic wind-hovering uavs," *Unmanned Systems*, 2022.

[18] ANSYS, "Ansys® academic research fluent, release 19.5.0," 2019.

[19] Eclipson. 3d printed airplanes. [Online]. Available: https://www.eclipson-airplanes.com/modelc

[20] G. Hattenberger, M. Bronz, and M. Gorraz, "Using the paparazzi uav system for scientific research," 2014.

[21] Optitrack. Motion capture systems. [Online]. Available: http://www.optitrack.com/

II

Literature Study

2

Fundamentals of Soaring

This chapter provides an overview of the different types of soaring that exist. All soaring techniques aim to extract sufficient energy to stay airborne without losing altitude. If the soaring technique relies on a vertical, upward wind component we consider this static soaring. section 2.1 explains the theory behind static soaring. Its two most common types; thermal soaring and orographic soaring are explored in subsection 2.1.1 and subsection 2.1.2 respectively. If energy is instead extracted as a result of a gradient in the horizontal direction of wind, we consider this dynamic soaring. section 2.2 outlines the theory behind dynamic soaring.

2.1. Static Soaring

Before discussing the different types of static soaring, it is useful to define the dynamics involved. An overview of the kinematics is presented below using a point mass model. [2]

Define the vehicle mass m, angle of attach α and thrust, drag and lift force as T, D and L respectively. Starting with the forces parallel and perpendicular to the flight path we obtain:

$$mgcos(\gamma) = L + Tsin(\alpha) \tag{2.1}$$

$$mgsin(\gamma) = D - Tcos(\alpha) \tag{2.2}$$

Define the flight path angle γ, which is assumed small, proceeding with the small angle approximation.

$$mg = L = \frac{1}{2}\rho v_a^2 S C_L \tag{2.3}$$

Therefore:

$$C_L = \frac{2mg}{\rho v_a^2 S} \tag{2.4}$$

With C_L the lift coefficient, ρ the air density, v_a the airspeed and S the wing surface area. A second order approximation can then be given for the drag force.

$$D = \frac{1}{2}\rho v_a^2 S(a_0 + a_1 C_L + a_2 C_L^2) \tag{2.5}$$

Substituting this is Equation 2.2, the flight path angle for a given speed and thrust can be computed as:

$$mg\gamma = \frac{1}{2}\rho v_a^2(a_0 + a_1 C_L + a_2 C_L^2) - T \tag{2.6}$$

We can now consider the aircraft kinematics in terms of the airspeed, flight path angle and the wind speed. We define $\dot{x}_i$ as the horizontal velocity component and $\dot{z}_i$ as the vertical velocity component in the inertial frame. the wind speed is modelled as a polynomial function of the position in the inertial frame: $w = f(x_i, z_i)$. We obtain:

$$\dot{x}_i = v_a cos(\gamma) + w_x \tag{2.7}$$

$$\dot{z}_i = v_a sin(\gamma) + w_x \tag{2.8}$$

Note that for this derivation we use the maintain the assumption that the aircraft is in equilibrium. This assumption is only adequate if we consider the flight as segments of constant airspeed.

2.1.1. Thermal Soaring

The density of air decreases with an increasing air temperature. Due to this, volumes of warmer rise and form local updrafts. Differences in this air temperature can mainly be attributed to the uneven heating of the ground surface. Thermal soaring is a static soaring technique that uses these thermal updrafts [3].

The technique is commonly used by gliders and birds. In the air sport of gliding, the manoeuvres to fly and circle into the thermals are done manually by the pilot. In manual flight, thermals are usually found by the indication of cumulus clouds at the top of the thermal. Thermals can also be formed along a line, creating horizontal convective rolls. [4] Glider pilots can use this phenomena to fly straight for long distances, hence the colloquial name: cloud streets. A schematic comparison of both types of thermal updrafts is shown in Figure 2.1.

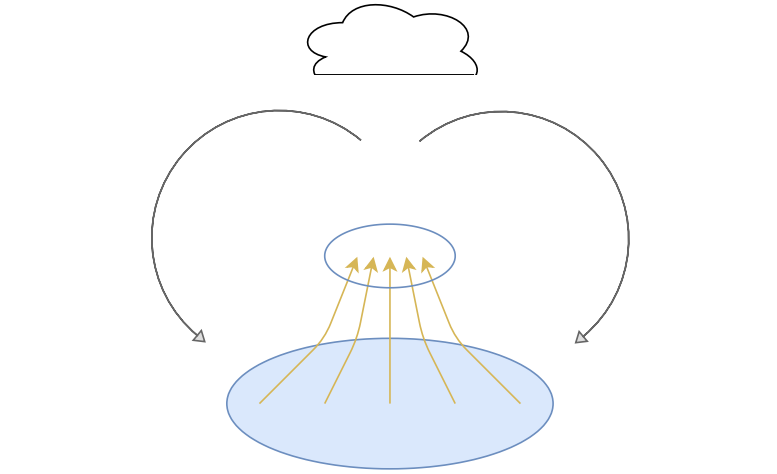

(a) Local Thermal Updraft

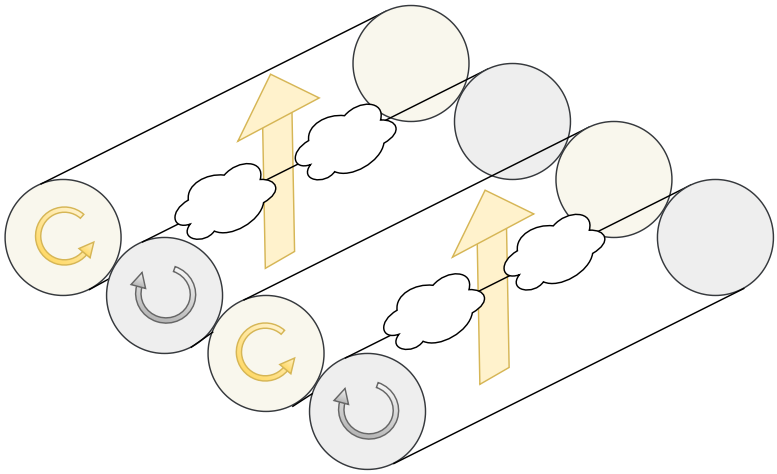

(b) Horizontal Convective Rolls

Figure 2.1: Local Thermal Updraft VS Horizontal Convective Rolls

A much researched field in academia is the detection of thermals in real time, enabling the possi-

bility to fly through them autonomously. Allen [5] presented an algorithm to detect thermal updrafts based on aircraft acceleration and pressure changes. In a simulated environment fed with historical meteorological data, the solution is successful in soaring autonomously.

Dunn et al. [6] and Woodbury et al. [7] have performed research in the use of reinforcement learning to guide UAV's towards thermals. Simulations have shown promising results, converging to a thermal in over 85% of the cases. Efficient path planning by leveraging thermals has been studied by Khaghani [8] and Akos [9]. Various control strategies and simulation improvements have been proposed with observations confirming the generality and applicability of leveraging thermals for efficient flight. It is worth noting that practical tests and results are mostly lacking in this field.

2.1.2. Orographic Soaring

Orographic soaring is the subset of static soaring where the updraft is generated by the upwards deflection of the wind stream by large objects. An example of orographic updraft is ridge lift on the windward side of a hill or slope, as illustrated in Figure 2.2. Horizontal flow is deflected by the hill, resulting in a vertical wind component.

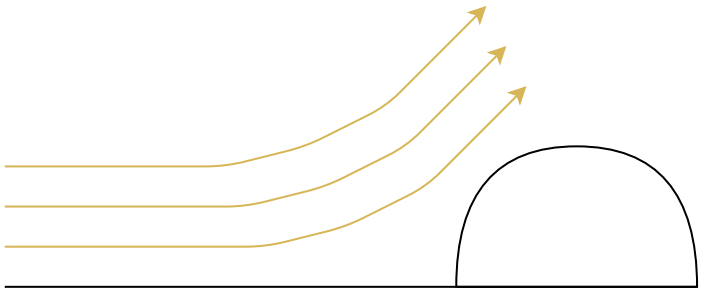

Figure 2.2: Ridge Lift

Next to the origin of the updraft itself, another important difference between thermal and orographic updraft needs to be considered. For orographic soaring, a horizontal wind component is necessary for technique to be viable. For the environmental conditions, this means that there is at least mild wind at the flying site. Because of this, wind speed is a significant contributor to the vehicles airspeed. Ground speed can not be used as a reliable metric for heading and airspeed and state estimation becomes a bigger challenge. A circling manoeuvre is also more difficult because of the wind. This is in contrast to thermal soaring. For this method, no horizontal wind speed component is needed. In fact, thermal updraft is usually present on wind calm days. The environmental conditions to make both static soaring techniques viable are therefore very different. [10]

In comparison with thermal soaring, there is also significantly less research available on orographic soaring. A possible cause for this is that good conditions for orographic soaring are much more constraining. Wind needs to come from a suitable direction relative to the deflection object. Furthermore, these objects need to be positioned along the desired flight path.

The possible use case of flying in the updraft generated by buildings is being researched at the Royal Melbourne Institute of Technology (RMIT). White et al. [11] proved the feasibility of soaring in urban environments. In their study, full-size building results and 1/100th scale wind tunnel tests agreed on the measured vertical velocity components. This vertical components was found to be 15% - 50% of the mean wind velocity at the building's height. The study concluded that this region, immediately upwind of the building, the updraft is sufficient for MAV's with a sink rate below 0.5 m/s. A follow up paper notes that this region exhibited high turbulence intensities and controllability challenges need to be overcome. [12] Also at RMIT, Mohamed et al. [13] have researched a turbulence mitigation system for MAV's. The proposed phase-advanced sensory system shows significant improvements compared the disturbance rejection performance of standard inertial-only control system.

Fisher et al. [10] expanded on the work of White et al. by creating a control algorithm to enable

autonomous soaring. Two different cases were analysed; the wind field over a hill and the wind field over a building. Real flight testing in the hill case proved consistently successful in soaring for extended duration, with battery capacity for the on-board electronics being the next constraint on flight time. Flights around a building could not be sustained for more than approximately 20s. This was attributed to significant gusts in the oncoming wind, effectively nullifying the vertical updraft component for a sustained period.

Finally, past research in this field has been performed at Delft University of Technology (TU Delft). The first wind field that was studied is the case of soaring along dunes. Secondly the feasibility of soaring in the updraft generated by a moving object was studied. For this case, tests were performed with a ship in open sea and a Parrot Disco UAV. The study presents a controller capable of autonomous soaring and the tests proved the feasibility of soaring over dunes and at the windward side of a moving ship in open sea. Further research is suggested in more robust geolocation systems and positioning accuracy. Particularly methods to obtain accurate heading information when soaring with near zero ground speed. Furthermore, performing more practical flight tests in a wide variety of wind conditions is recommended [14].

2.2. Dynamic Soaring

Dynamic soaring extracts energy from a wind gradient in the horizontal direction. In contrast to static soaring, this soaring technique does not rely on a vertical wind component. This section will outline the mechanisms making dynamic soaring possible and discuss the relevant literature published in this field.

The main mechanism behind dynamic soaring is best explained as a repeating cycle with intermediate steps. We first consider the aircraft flying in a stationary volume of air. At this moment, the ground speed and airspeed are identical. The aircraft then proceeds to enter a moving mass of air head-on. The ground speed of the aircraft will remain nearly the same while this manoeuvre causes the airspeed to increase momentarily. The aircraft will now perform a 180^o turn, due to the conservation of its momentum, the aircraft is able to maintain most of its increased airspeed. At this point, the aircraft is travelling downwind with an increased airspeed. The effective ground speed has therefore increased. The cycle can be repeated by piercing the boundary layer again to the stationary volume of air. The aircraft will maintain its' -now increased- ground speed. Another 180^o turn can be performed in the stationary volume of air to reach the starting point with a higher speed compared to the start of the cycle. While drag forces continuously reduce the airspeed of any aircraft, the cycle can be repeated quickly enough to make up for this loss and therefore allowing the aircraft to stay airborne indefinitely. [15]

The cycle is shown in Figure 2.3.
It is worth noting that instead of a hard boundary layer as depicted in Figure 2.3, a wind gradient also allows for dynamic soaring. Furthermore, a Dynamic soaring cycle does not necessarily have to start and end in the same spot. Instead it is also possible to traverse half circles in opposite directions. A slalom flight can be performed by climbing through the wind gradient and facing an increasing wind component. The cycle is then completed by turning downwind again and descending along the decreasing wind gradient. Note that this manoeuvre is most effective when travelling perpendicular to the wind direction. A graphic representation of this manoeuvre is shown in Figure 2.4.

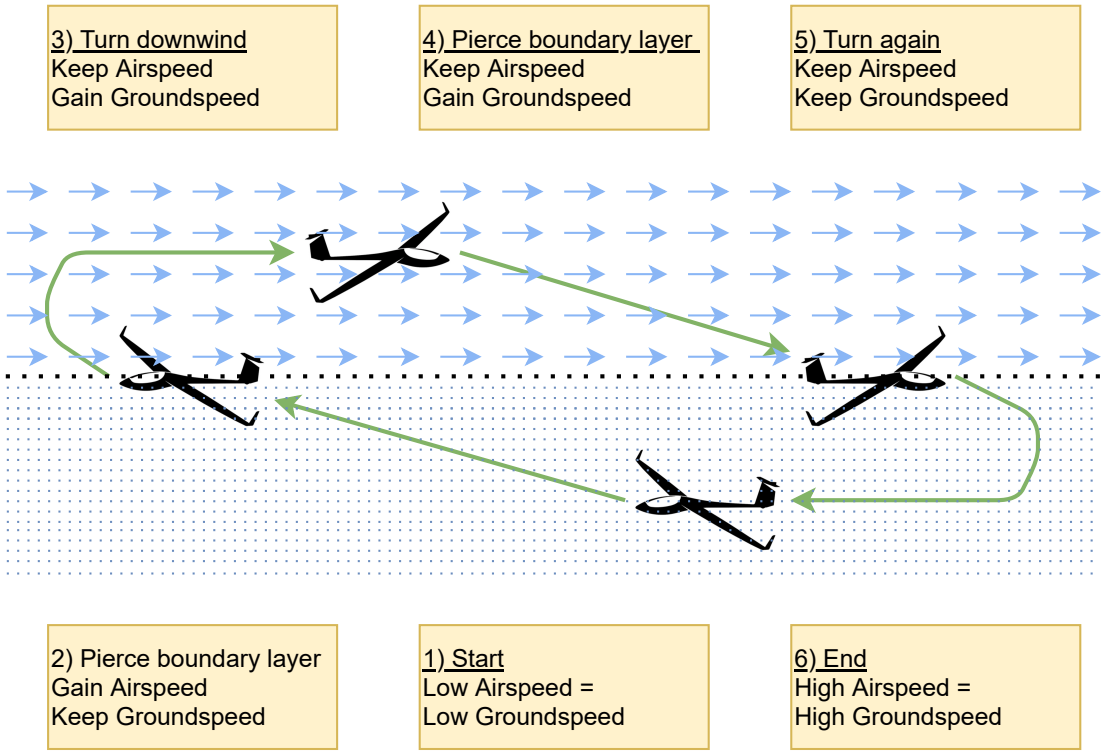

Figure 2.3: Dynamic Soaring Cycle Steps

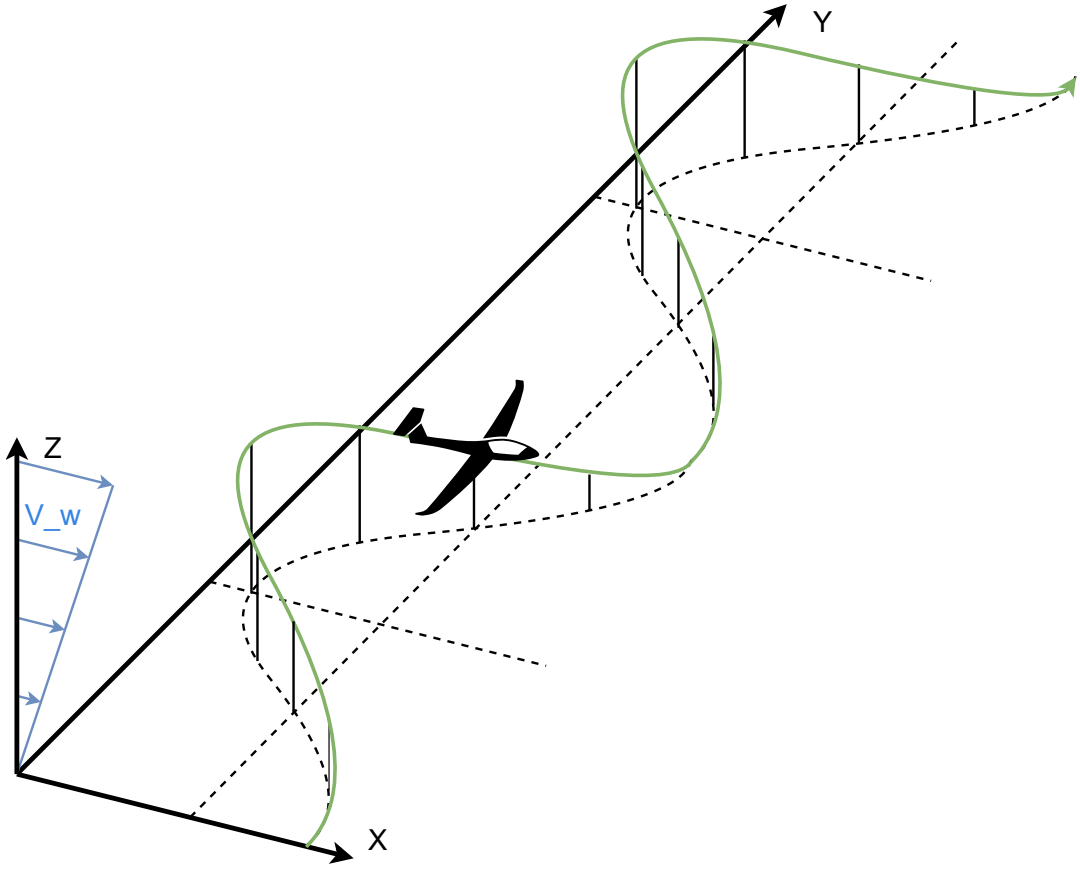

Figure 2.4: Dynamic Soaring Flight Path

Particularly albatrosses have perfected the technique of dynamic soaring. They have shown the ability to travel incredible distances while using very little energy. The first mention of dynamic soaring was in 1883 by Lord Rayleigh in Nature [16]. In this work he concluded that in a horizontal wind field, soaring would only be possible if the wind is not uniform. Further research on the topic mainly focuses on the generation of a flight path exploiting dynamic soaring along a desired flight direction.[17] [18]

3

Soaring Windfield

In order to develop the autonomous control behaviour of an UAV, it is helpful to have a model of the wind field over an obstacle in a simulated environment. Through this, wind field parameters can easily be adjusted and insight can be gained in the UAV performance characteristics.

3.1. Wind Field Estimation

Various methods exist to estimate the wind field, each with their own advantages, level of complexity and computational demand. This section presents an overview of common techniques.

3.1.1. Computational Fluid Dynamics

An accurate approach in estimating a flow field is through computational fluid dynamics (CFD). CFD can be seen as the group of computational methodologies used to solve the equations that govern fluid flow. [19]. Usually this is done through solving numerous Navier-Stokes equations. A prerequisite for the analysis is the process of meshing, where the geometry is sliced in a large finite set of grid points. The resolution of this meshing process can vary, based on the required accuracy and computation power available. Secondly, initial conditions have to be carefully selected each time a simulation is ran. The obtained results can be very accurate but the process of setting up and/or changing the conditions of a simulation is tedious and time consuming.

3.1.2. Potential Flow

Langelaan [2] [20] used a simplified potential flow method for the estimation of the wind field over an idealised hill with a semi-circular cross section. Potential flow theory has a few limiting assumptions which are summarised below [21].

- Incompressible: potential flow reduces to a simple system that can be analyzed using complex analysis when the flow is incompressible. This is the case for low Mach numbers (M<0.3).
- Irrotational: Assumes a curl-free vector field where the vorticity of the flow is zero.
- Inviscid: Assumes that the flow has viscosity of zero. Practically, this assumption dictates that no flow separation occurs.

Given these assumptions, potential flow can be concluded as a valid method for wind field estimation when these limitations are respected. In the analysis we are mainly interested in the deflection of a uniform wind stream on the windward side of an object. Given the low wind speed and that no flow separation occurs, this can be modelled with potential flow theory. [22]

We can now consider the potential flow around a cylinder. This can be obtained by considering a uniform stream of velocity (U) and a doublet at the center of the cylinder such that the stagnation point precisely matches the boundary of the cylinder. The solution is most easily obtained in polar coordinates:

$$\Phi(r,\theta) = Ur(1 - \frac{R^2}{r^2}cos(\theta) \tag{3.1}$$

The velocity in polar coordinates is then:

$$V_r = \frac{\delta\Phi}{\delta r} = U(1 - \frac{R^2}{r^2}cos(\theta)) \tag{3.2}$$

$$V_\theta = \frac{1}{r}\frac{\delta\Phi}{\delta\theta} = -U(1 + \frac{R^2}{r^2}sin(\theta)) \tag{3.3}$$

This can be related to Cartesian coordinates by substituting $x = rcos(\theta)$ and $y = rsin(\theta)$. Since the flow is inviscid and irrotational, Bernoulli's equation allows to directly solve the pressure field after the velocity field is calculated:

$$\rho = \frac{1}{2}\rho(U^2 - V^2) + \rho_\infty \tag{3.4}$$

The resultant velocity and pressure field around a cilinder is illustrated in Figure 3.1. Note that red denotes a high pressure region and blue a low pressure region.

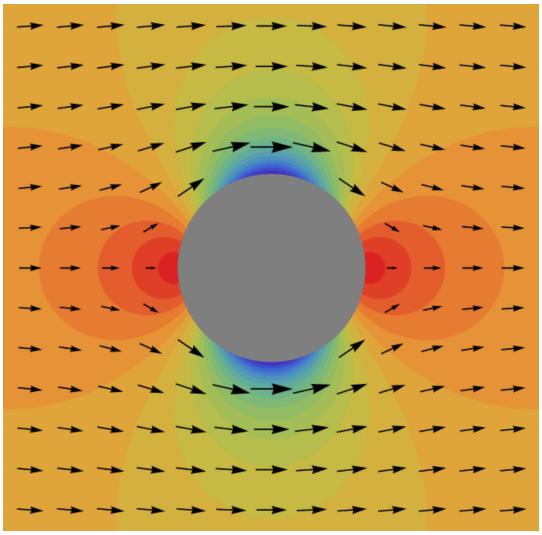

Figure 3.1: Potential Flow Around a Cylinder

The flow around a cylinder is of interest since the upper left quadrant of this velocity field can be used as a simplified wind field estimation on the windward side of a smooth object such as a hill.

3.2. Soaring Feasibility Region

In a given wind field it is useful to consider the vertical component of the flow. Since this research considers orographic soaring, rising air is the mechanism through which soaring is realised. Therefore, the vertical updraft has to be at least equal to the minimum sink rate of the aircraft. In Figure 3.2, the vertical updraft component over a 2D hill is plotted.

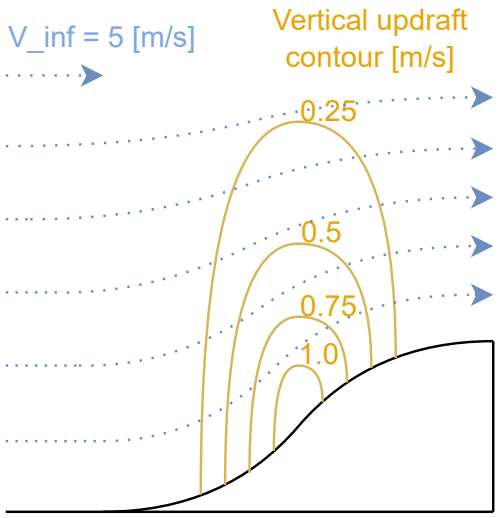

Figure 3.2: Vertical updraft component in orographic wind field.

It can be observed that the highest updraft is near the surface, halfway up the hill and it decreases continuously when moving further from the center. This flow field is typical for the majority of cases of orographic lift. The fact that there is a continuously decreasing updraft in the wind field is an important property for control techniques explored in chapter 4.

Furthermore, it should be noted that the required updraft to stay airborne is a function of the vehicles airspeed. To stay stationary while soaring, the sink rate of the aircraft has to equal the updraft at its soaring location in the windfield. If the updraft exceeds the sink rate there is an excess updraft and vice versa. At the maximum endurance speed (V_{ME}) a particular airframe will experience the lowest rate of sink. At lower velocities the airfoil will enter its stall regime and sink rate will increase. To maintain higher velocities than V_{ME} during unpowered flight, the aircraft has to assume a nose down attitude and the sink rate will increase as well. The glide polar of a given airframe can be approximated with a quadratic function. An approximate glide polar for a given airframe is shown in Figure 3.3

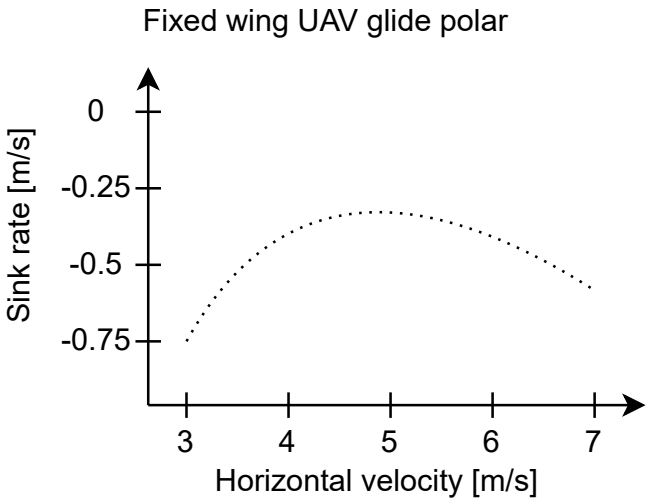

Figure 3.3: Generic glide polar of a fixed wing UAV.

The glide polar defines the relation of the sink rate and horizontal velocity. Mapping of this glide polar on the orographic wind field yields the zero excess updraft contour. At every point in the wind field, the local vertical updraft component is compared to the expected sink rate at the local horizontal wind

velocity according to the glide polar. The zero excess updraft contour is defined by this comparison, where the inner region shows excess updraft and the outer region a lack of sufficient updraft. The process is illustrated in Figure 3.4 , where a single contour line can be seen where the local sink rate equals the local updraft. For illustration the contour with $0.25[m/s]$ excess updraft and a $0.25[m/s]$ lack in updraft are shown as well.

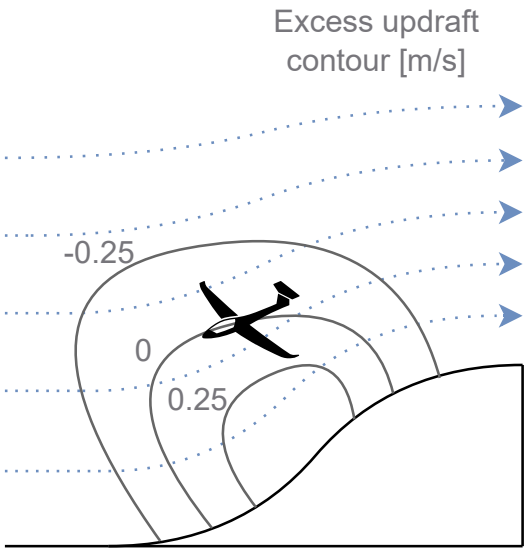

Figure 3.4: Constant excess updraft regions and the zero excess updraft contour.

4

Control Algorithms

This chapter discusses the relevant literature related to the control aspects of autonomous orographic soaring. In section 4.1 the constraints on control freedom while soaring are explored. section 4.2 outlines the concept of a total energy control system. Both of these subjects are necessary background to explore different control strategies in section 4.3.

4.1. Control Freedom

This section covers the degree of control freedom (DOF) that is possible while soaring. We consider traditional fixed wing dynamics with actuator control for throttle, elevator, rudder and aileron. With the aim of reducing or restricting throttle usage while soaring, the longitudinal dynamics are affected. In this section we therefore consider a 3 degrees of freedom representation with position given by X and Z, and pitch angle θ. Effective actuators are thrust δ_t and elevator deflection δ_e.

In this case we can note that using both throttle and elevator control, 2 degrees of freedom can be realized. In Figure 4.1 it is illustrated that full control in $\dot{X}$ and $\dot{Z}$ is possible at the expense of θ, which is now fully dependent variable. Similarly, for a given pitch θ the throttle level can still dictate the flight path. As shown, varying the airspeed will result in a different flight path. However, $\dot{X}$ and $\dot{Z}$ can not be independently controlled.

It is worth analyzing what happens in case the throttle level is set to a fixed value. In this case a trajectory can still be followed but $\dot{X}$ and $\dot{Z}$ are dependent on each other. Since they can not be controlled individually, effectively 1 DOF remains. Similarly, in the case of a fixed throttle it is still possible to command given pitch θ. However, this is at the expense of any control in $\dot{X}$ and $\dot{Z}$ which are now fully dependent variables.

Note that above analysis is only valid within the operational envelop of the aircraft. Limitations in performance and control authority can further decrease the effective control authority available. This limited control authority is important when considering the case of soaring, since ideally no throttle input is used. This is further expanded upon in section 4.3.

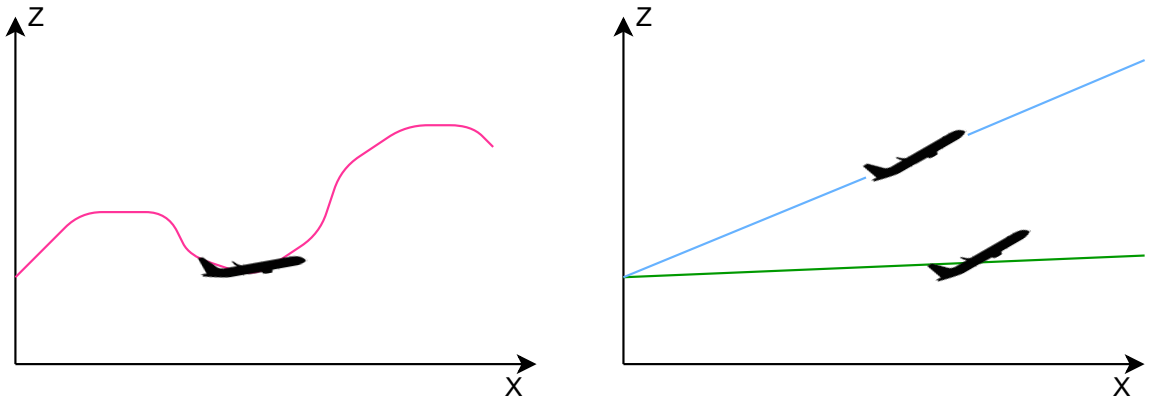

Defined trajectory along X and Y

Throttle and Elevator authority
- Full freedom in $\dot{X}$, $\dot{Y}$
- θ is dependent on trajectory, cannot be controlled

Only Elevator authority
- $\dot{X}$ and $\dot{Y}$ are dependent on each other, cannot be controlled individually
- θ is dependent on trajectory, cannot be controlled

Defined θ

Throttle and Elevator authority
- Full freedom in θ
- $\dot{X}$ and $\dot{Y}$ are dependent on each other, cannot be controlled individually

Only Elevator authority
- Full freedom in θ
- $\dot{X}$ and $\dot{Y}$ are fully dependent, cannot be controlled

Figure 4.1: Comparison in the longitudinal motion with and without throttle control.

4.2. Total Energy Control

A total energy control system (TECS) is a longitudinal flight control concept. It aims to solve to limitations of conventional auto throttle and pitch autopilot control systems. Separate control logic for these quantities is inherently suboptimal due to the highly coupled longitudinal flight path and speed response of aircraft. At it's core, a TECS controls the energy state of the system, comprised of its kinetic and potential energy. The thrust command is computed from the projected energy demand based off the flight path target and speed target. The elevator command is calculated from the energy balance error between the flight path and velocity. [23]. Note how TECS are useful to study in the context of soaring since it also requires delicate control of the aircraft's total energy and energy balance.

We define the total energy of the aircraft as the sum of its kinetic and potential energy:

$$E_t = E_p + E_k \tag{4.1}$$

$$E_t = mgh + \frac{mv^2}{2} \tag{4.2}$$

When taking the derivative with respect to time, the total energy rate is obtained. [24]

$$\dot{E}_t = mgh + mv\dot{v} \tag{4.3}$$

We can now define the specific energy rate as:

$$\dot{E} = \frac{\dot{E}_t}{mgv} = \frac{\dot{v}}{g} + \frac{\dot{h}}{v} = \frac{\dot{v}}{g} + sin\gamma \tag{4.4}$$

We can substitute this in the horizontal dynamic equations of an aircraft

$$mg\frac{\dot{v}}{g} + sin\gamma = T - D \tag{4.5}$$

In trimmed level flight, initial thrust equals the drag force. For a small flight path angle: $sin\gamma = \gamma$. Therefore:

$$\Delta T = mg\frac{\dot{v}}{g} + \gamma \tag{4.6}$$

It is evident that ΔT is proportional to $\dot{E}$ so the thrust set point should be used as the quantity to control total energy.

Elevator control conserves the total energy and can be used to exchange potential and kinetic energy. In this control structure we define the specific energy balance rate as follows:

$$\dot{B} = \gamma - \frac{\dot{v}}{g} \tag{4.7}$$

Figure 4.2 shows a simplified control diagram of a TECS. [24] [25]

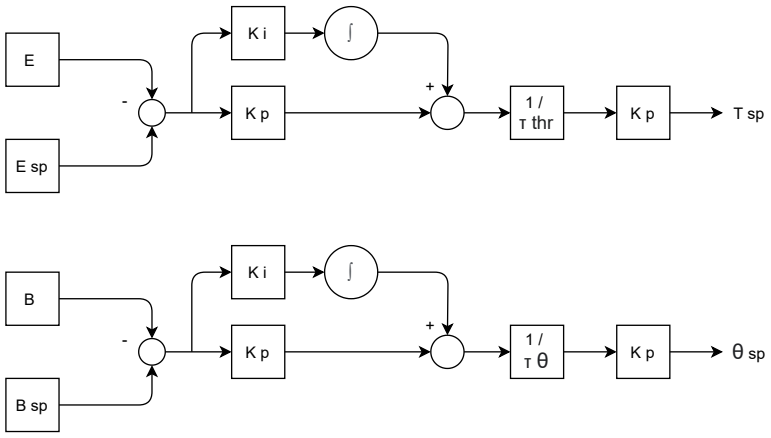

Figure 4.2: Total Energy Control System Diagram

For the case of orographic soaring, we can readily calculate the total energy as a function of wind speed and airspeed. [2] [20]

$$E = E_p + E_k \tag{4.8}$$

$$E = mgh + \frac{m(\dot{x}_i^2 + \dot{z}_i^2)}{2} \tag{4.9}$$

Substituting the vehicle kinematics derived in section 2.1, we obtain:

$$E = mgh + \frac{1}{2}m((v_a cos(\gamma) + w_x)^2 + (v_a sin(\gamma) + w_z)^2) \tag{4.10}$$

Resulting in the following equation for total energy:

$$E = mgh + \frac{1}{2}m(v_a^2 + 2w_x v_a cos(\gamma) + 2w_z v_a sin(\gamma) + w_x^2 + w_z^2) \tag{4.11}$$

4.3. Control Strategies

This section considers different control strategies to realize autonomous soaring. Specifically, we are seeking the case where the primary forces on the aircraft balance and its velocity is zero. Furthermore, the aircraft throttle should be zero while soaring. In Figure 4.3 an illustration is given of this case: $L + D + W = 0$ The aircraft velocity vector is equal direction but opposite in magnitude to the local wind field vector: $v = -w$. The aircraft is at rest with zero ground speed.

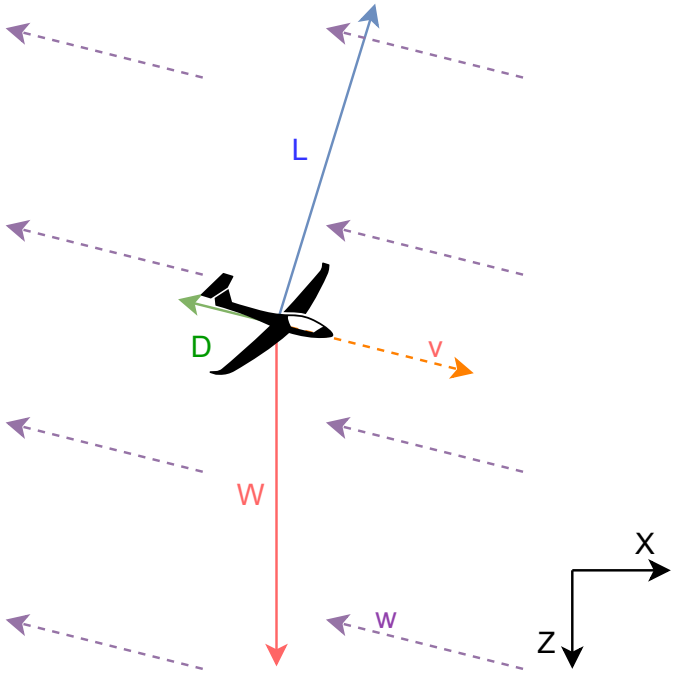

Figure 4.3: Soaring force and velocity equilibrium.

This delicate balance is only possible when the updraft matches the required updraft. At this point, the local wind field vector is exactly opposite to an airspeed vector that is compatible with a trimmed flight condition where the primary forces cancel out. As outlined in chapter 3, a typical wind field suitable for orographic soaring will have a continuously decreasing updraft. If the maximum updraft in the wind field is higher than the required updraft for a particular airplane, it can be expected that orographic soaring is possible on one of the updraft contours.

For any given updraft gradient line in the wind field, there is one point where the forces would balance to allow for stationary orographic soaring, as shown in Figure 4.4. Following from section 4.1, full position control authority is not possible in this wind field without throttle use. With the right control strategy, moving along the updraft contour should however be possible.

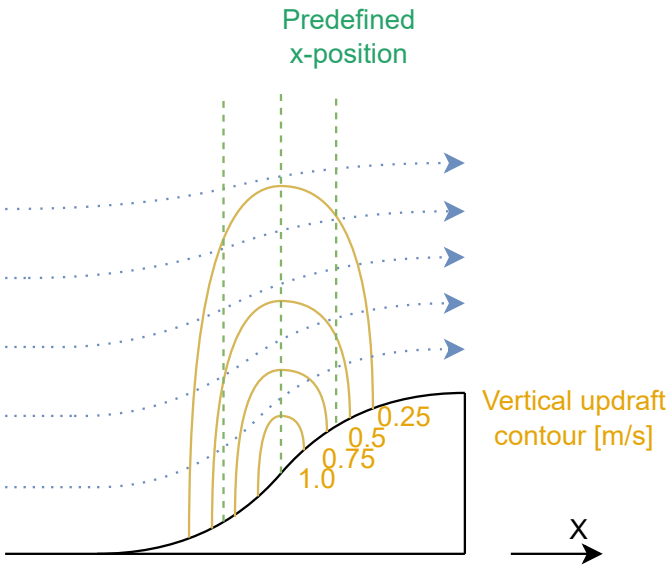

Figure 4.4: Orographic wind field at predefined X positions.

In their studies on orographic soaring, Fisher et al. [10] used a position controller in which the x-position error was used to generate pitch commands. The limitations of this design were that the controller could only be enabled when the aircraft was already flying in the soaring feasibility region. Furthermore, the target x-position needs to be carefully chosen as such that the a downstream drift results in an increase in updraft and vice versa. Notice in Figure 4.4 how this is not always to case when a vertical gradient is located further downstream. The controller diagram is shown in Figure 4.5 A separate lateral controller was used taking into account the y-position error to keep the aircraft aligned and facing directly into the wind.

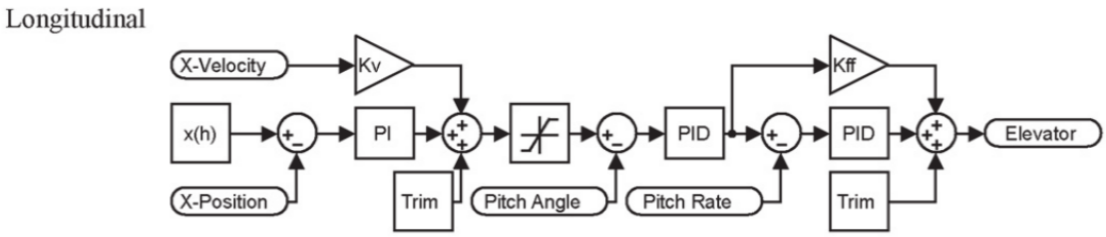

Figure 4.5: Soaring Controller Fisher et Al

C. de Jong et al. [14] used the Paparazzi TECS and added an outer loop controller. A position error in x was fed into a PI controller to compute an airspeed setpoint that is fed into the TECS. Through this, a target position can be maintained. Solely the kinetic energy is fed through the throttle. By setting very low gains the throttle is only used when critical and the aircraft is nearing stall behaviour. The lack of potential energy error input to the throttle means it won't kick in when the aircraft loses altitude while soaring. The controller is presented in Figure 4.6.

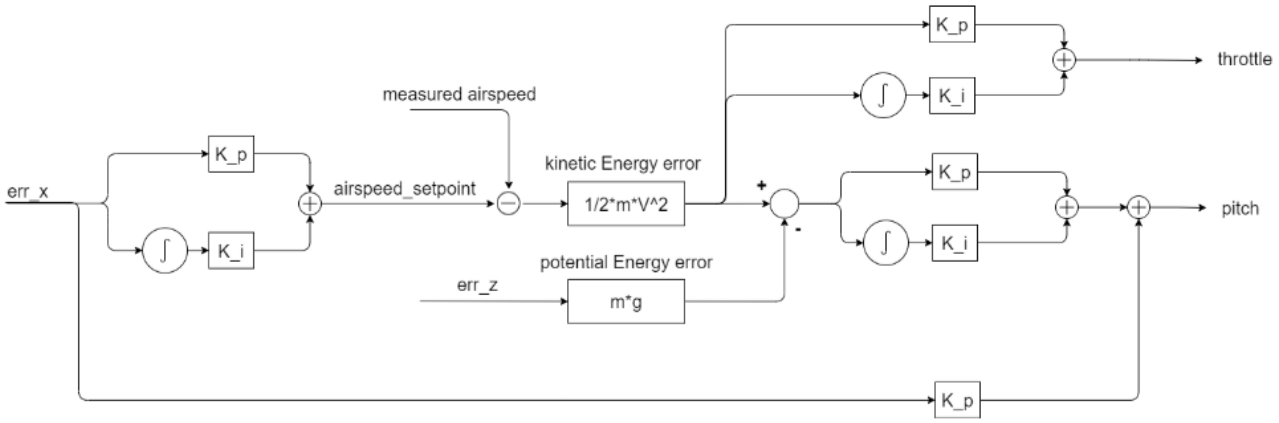

Figure 4.6: Soaring Controller De Jong et el.

Preliminary research on this topic has shown that a pitch controller based on the tangent position error to an updraft potential gradient is effective. When a diagonal gradient is chosen, the controller is quite robust in converging to a stable soaring position on this gradient. An example of such gradient would be the diagonal line in Figure 4.4.

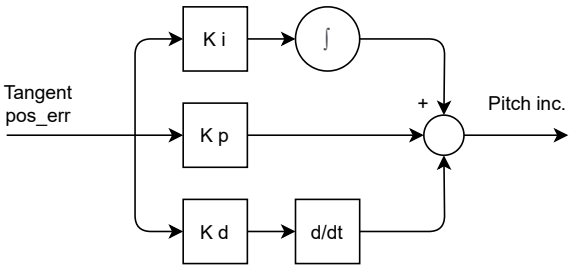

Figure 4.7: Tangent Error Pitch Control

Letting a controller converge to a line rather than a single point in the vertical plane addresses the limited control freedom of an aircraft that has no propeller and can only effect its longitudinal motion by elevator deflection. A single degree of position control can be achieved by moving the target gradient up or down along Z or changing the angle of the gradient. Through this, the aircraft can track the gradient along its zero excess updraft contour.

5

Attitude and Positioning Systems

In order to realise the goal of autonomous soaring, a reliable means of obtaining the orientation of the vehicle is needed. We distinguish the need for a positioning system and attitude determination system. section 5.1 defines the performance metrics that are used in this comparative assessment. section 5.2 outlines the comparison of various relevant positioning systems and attitude determination systems.

5.1. Performance Assessment

When comparing the performance of position- and attitude determination systems, it is important to establish relevant metrics on which to form a base of comparison. In this section we define the following metrics: accuracy, precision, robustness and coverage. These are deemed of the highest importance for the project.

Accuracy

The most important metric to consider is the accuracy of the system. The Joint Committee for Guides in Metrology has defined accuracy as the measure of the degree in closeness of a given measurement to its true value [26]. Practically, in the case of a positioning system, the accuracy refers to the distance between the measured position and true position. Likewise, in the case of attitude determination, the accuracy is the difference between the measured angle and true angle. In case multiple measurements are considered, the accuracy can be computed by taking the mean of the measurements.

Precision

Closely related to accuracy, precision is a measure of the consistency of the measurements. It reveals insight in the variation of performance over multiple samples. It possible for a positioning system to be precise if all measurements are closely clustered together, even though the accuracy can be off by a consistent amount on each measurement. Similarly a system can be accurate but not precise if all measurements are sparsely clustered around the true value [26].

Robustness

Particularly interesting when researching soaring in complex environments is the robustness of the position and attitude determination. A system is said to be highly robust if it performs well in situations outside its expected scope. For example, when a position system still functions appropriately in the vicinity of large buildings or surfaces it is said to be robust against multi path effects.

Coverage

The coverage is the measure of the area in which a system can operate. In the case of heading estimation by magnetic compass, there is no coverage near the polar regions or near magnetic objects. In the case of UWB positioning, the coverage is highly dependent on the presence of additional hardware in its vicinity. We can differentiate local coverage, scalable coverage and global coverage [27]. With local coverage, the system is only intended to function in a small predefined area. Scalable coverage allows for the possibility to increase the covered area by installing additional hardware. Global coverage, by

definition, operates worldwide without the need to install additional hardware or modify the system.

It is worth noting that aforementioned performance metrics are usually not independent quantities. It is for example common for a system to trade off a loss of accuracy for an increase in coverage. Likewise, ensuring high robustness of a system is usually at the expense of coverage. It is therefore important to consider these performance metrics in the context of the intended use case of the system.

5.2. Attitude and Positioning Systems

This section outlines multiple positioning systems that are worthwhile researching in the context of autonomous soaring.

Global Navigation Satellite System

The first positioning system to be considered are Global Navigation Satellite Systems (GNSS). This system relies on signals from orbiting satellites where a small electronic receiver can provide geo-spacial positioning data. Four main satellite systems can be identified for this purpose; GPS, GLONASS, Beidou and Galileo. These systems are owned and ran by the United States, Russia, China and Europe respectively, though they each provide global coverage and public use. Clock drift, ephemeris, ionospheric delay and multi-path effects are contributing factors that can negatively impact the accuracy and reliability of the system. These attributes can be improved by utilising a GNSS augmentation system. These systems usually rely on ground based stations and can improve the systems attributes in the regions they are active. Examples of such systems are EGNOS in Europe and WAAS in North America. Multi-path effects and errors can be combated by using two frequency bands of a GNSS system simultaneously. Though the exact performance and specifications of the 4 Major GNSS vary, an accuracy of around 1 meter can be expected in good conditions. It is worth noting a majority of GNSS receivers support multiple GNSS systems simultaneously, which can further improve the accuracy, precision, coverage and robustness.

Real Time Kinematics

Real Time Kinematics is a technique that can further enhance the satellite based positioning systems. Conceptually, it is similar to the augmentation technique discussed in section 5.2 but deployed at a much smaller and more local scale. In a typical RTK setup, a base station considers the carrier wave of the satellite signal it receives. The base station then broadcasts the phase of the carrier it received. Mobile units can compare this with the own phase they observed. This allows the system to obtain a relative accuracy of around 1 cm. It is worth noting that this the absolute accuracy of the system is not enhanced and depends on how well the position of the ground station is known.

Multi-Antenna GNSS

Another variation on GNSS positioning is the use of a multi-antenna GNSS receiver. In this setup, a mobile array is used in which 2 or more GNSS antennas are relatively fixed. The distance between the antennas will result in a slight difference in the received signals. The difference in the total phases of the carrier signal is then used to resolve attitude information. A common setup uses a dual antenna receiver. Through this the heading can be resolved as well as one other primary attitude angle. It is wise to orient the antennas as such that the heading can be resolved through all stages of flight; e.g. for a tail sitter aircraft the antennas can be placed at each wingtip so the heading is resolvable in the upright state as well as forward flight.

Ultra Wide Band

Ultra Wide Band is a wireless technology reliant on radio waves. UWB allows for the transmission of large amounts of data over short ranges. It employs a wide frequency spectrum of at least 500 MHz with the center frequency in the 3.3 to 10.4 GHz range. Through measuring the Time-of-Flight, UWB can be used in a real time location system, generally in a peer-to-peer configuration. Advantages of the system include its low power consumption and suitability in radio frequency sensitive environments. Positioning performance varies depending on the setup and application. When deployed correctly, an accuracy of at least 50cm can be expected.

Bluetooth and Wireless LAN

Bluetooth and WLAN are wireless communication standards for exchanging data. Both operate in the UHF spectrum at a frequency around 2.4GHz. The range of both systems rarely exceeds 50m. Through the Cell of Origin or triangulation method, localisation is possible inside a WLAN or Bluetooth network. These techniques rely on a perceived signal strength indicator (RSSI) to estimate position. This makes the system inherently susceptible to signal attenuation and the resultant accuracy is quite poor. Existing infrastructure is common and widespread, therefore the additional cost and hardware for a setup is often minimal.

Infrared Localisation

Infrared localisation is a technique that relies on the Time-of-Flight of an infrared signal with a unique ID. In the most common implementations, an on-board transmitter on the target is continuously broadcasting this signal. Through the use of multiple receivers, a position can be estimated quite accurately. A limitation of this system is that is relies on a clear line of sight between transmitter and receiver. Infrared localisation does not rely on- or interfere with electromagnetic waves outside the IR spectrum.

Optical Motion Capture

Optical motion capture is a positioning technique in which multiple synchronized cameras capture 2D images of the target from different angles. Through software, a 3D fix can be calculated by the overlapping and comparing positioning data. IR LEDs illuminating the target combined with small reflectors on the target can aid in this process. Since the systems relies on visible or IR light, a clear line of sight between the target and receiver is necessary.

Dead Reckoning

Dead Reckoning is a positioning technique where the position is estimated based on a previous known position and the elapsed speed and acceleration over time. Usually the velocity is obtained through integrating the acceleration measurements. Subsequently integration of the velocity yields the position estimate. The use of inertial navigation systems which provide very accurate directional information make the technique quite accurate, especially within short time frames. For longer durations, the method is prone to accumulating errors and drift. As a result, dead reckoning is usually combined with other position methods. As such, higher frequency measurement errors of other systems can be kept between bounds while long term drift can be corrected. Kalman filters are most commonly used in algorithms to obtain this.

5.3. System comparison

In Figure 5.1, an overview of the systems discussed in section 5.2 is given. The systems have been organised based on their mode of operation and the type of data they are able to provide. In Table 5.1, a comparison of the performance metrics of each position system is given. System precision was found to be very hardware dependent. Furthermore, literature on this metric was inconsistent. Since it does not provide meaningful insight in this comparison it was omitted from the table. However, the metric remains important when evaluating specific systems in the future of this project. it is worth noting that for all systems except those reliant on GNSS, that the accuracy is a relative metric. The absolute accuracy can never exceed the accuracy with which the position of the base station or beacons is know.

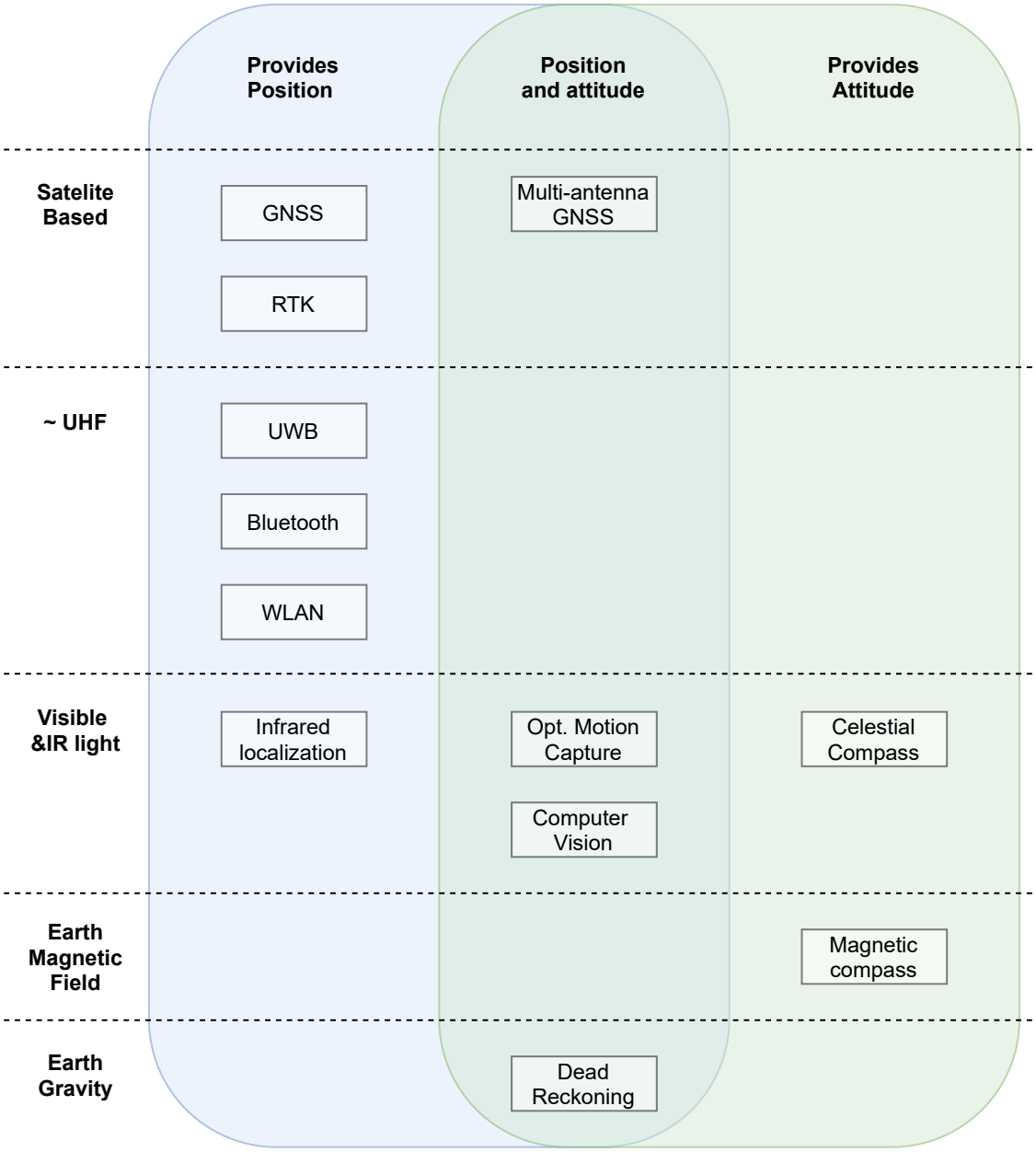

Figure 5.1: Positioning system comparison

Table 5.1: Positioning system comparison

System	Positioning (X,Y,Z - latt, long, alt)	Attitude (pitch, roll, yaw-heading)	Accuracy	Robustness	Coverage
GNSS (single antenna, augmented)	Yes	No	∼1 m	low	medium
Real Time Kinematics	Yes	No	∼1 cm	medium	low
Multi-antenna GNSS	Yes	Yes (#antenna dependent)	heading: <1 deg	medium	medium
Ultra Wide Band	Yes	No	∼1 cm	high	low
Bluetooth	Yes	No	1 - 10 m	low	low
WLAN	Yes	No	1 - 10 m	low	low
Infrared Localization	Yes	No	∼1 cm	medium	low
Optical Motion Tracking	Yes	Yes	∼1 cm	medium	low
Computer Vision	Yes	Yes	∼10 cm	low	medium
Celestial Compass	No	Yes (heading)	<1 deg	medium	medium
Magnetic Compass	No	Yes (heading)	∼2 - 10 deg	low	medium
Dead Reckoning	Yes	Yes	deteriorates	high	high

III

Further Analysis and Discussion

6

Dune Soaring

At the start of the thesis project, a manual soaring test flight was conducted at the Maasvlakte Beach. The dunes surrounding the Slufter create an ideal outdoor soaring environment during mild Southern or Westerly winds.

The goal of this soaring test flight was to obtain manual soaring flight and gather relevant position, attitude, pilot input and airspeed data. This data is later to be used to gain insight in the soaring dynamics of a fixed-wing UAV.

For this test, a 3D printed airframe was used, a scaled-down version of the same airframe that was later used for the indoor soaring experiments in the OJF. Note that the aircraft was equipped with a propeller in order to increase the manual control authority to find a suitable soaring position. In the soaring portions of the flight, the throttle setpoint was zero and the propeller was windmilling. The aircraft properties are tabulated in Table 6.1.

Table 6.1: Eclipson Model C Properties - Dune Flight

Wingspan	$770\ mm$
Length	$530\ mm$
Mass	$485\ g$
Wing Surface	$9\ dm^2$
Wing Loading	$53\ g/dm^2$
Stall Speed	$8.5\ m/s$
Maximum Speed	$20\ m/s$
Nominal Endurance	$45\ min$

With this emphasis on manual control and data gathering, it was opted to not use Paparazzi autopilot for this test. Instead, a control board running INAV was used [28]. The flight controller was setup for pure manual control, with all pilot inputs directly proportional to actuator deflections. The blackbox feature of INAV was configured to log the pilot inputs and aircraft attitude. Furthermore, a GNSS unit was attached to the controller to log position data. For a secondary source of altitude data, static air pressure was also measured and logged. The ability of INAV to be easily configured from a mobile phone reduced the complexity and overhead to conduct this test in a sandy and windy environment as compared to Pararazzi autopilot.

On the day of the test, there was a mild westerly wind of $10m/s$. The tests were conducted on a stretch of dunes that ran north to south, with the wind direction perpendicular to the dune face. In the soaring portions of the flight the pilot kept the throttle setpoint at 0. The pilot aimed to keep the wings level at all times using the appropriate roll input commands. Furthermore, it was aimed to maintain a heading directly into the wind using yaw input commands. Several soaring techniques where then examined.

Firstly, it was found that soaring flight could not be maintained passively with a tuned elevator trim setting. Unlike the aircraft roll attitude, where very little to no control input was needed to keep the aircraft level, the pitch attitude showed to be quickly diverging. As shown from multiple attempts, without

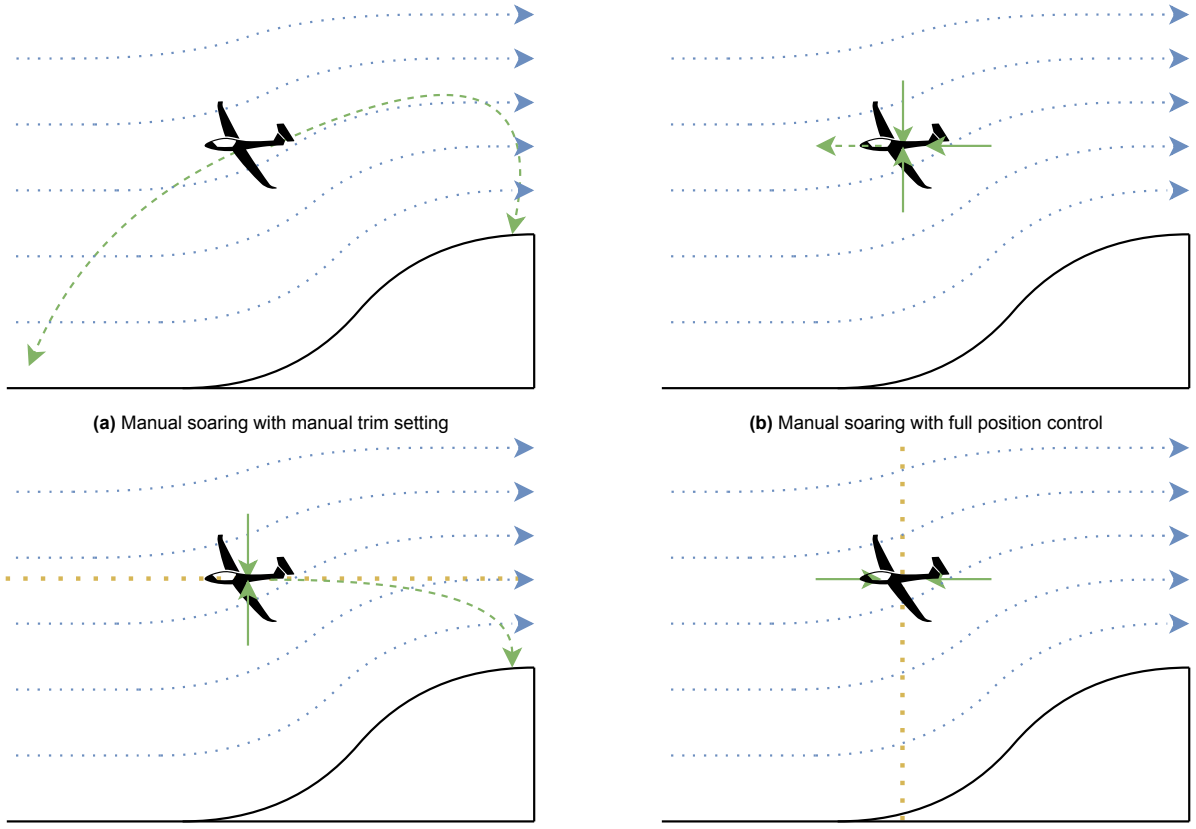

(a) Manual soaring with manual trim setting

(b) Manual soaring with full position control

(c) Manual soaring with constant altitude

(d) Manual soaring with constant X position

Figure 6.1: Four manual soaring flight experiments

intervention, the aircraft would either end up far downwind beyond the updraft region, or impacting the sand upwind. It was clear that an active control strategy is needed.

The second control strategy that was tested involved manually maneuvering the glider to a perceived good soaring location and attempting to maintain position control at that location. As theorized before the test flight, this was not possible without some throttle input at times. Adjusting the elevator deflection for pitch provided a fairly immediate response to maintain the desired altitude. However, it was not possible to maintain position along the longitudinal axis without using the throttle. When the aircraft drifted downwind from the desired soaring location, allowing some throttle usage proved effective. However, when the aircraft drifted upwind, not much could be done since the throttle setting cannot be moved below idle. To solve this limitation, we attempted to find a soaring location where a constant small, non-zero throttle input was needed to maintain position. This strategy would provide some available input range where the throttle could be reduced in case the UAV drifted upwind. This strategy was effective at maintaining position control. The mechanical energy cost of a constantly spinning propeller should be noted here as a drawback to this control method. However, at a suitable soaring location, this throttle usage is much less than what would be required to maintain steady flight in a regular, non-orographic windfield.

Thirdly, a control strategy was devised where the pilot aims to keep the altitude of the UAV constant using only pitch control. An approximate altitude which showed sufficient updraft during previous flight was chosen. This control strategy proved reasonably effective in maintaining soaring flight. An apparent problem while testing this strategy was that the UAV showed large displacements in the horizontal plane. From the perspective of the pilot it was therefore difficult to judge a constant altitude throughout the whole flight. During tests, the UAV had the tendency to drift down steam to over the top of the dune where it would experience more turbulent air and a lack of updraft causing the flight to be aborted. In later review, the flight logs showed that a constant altitude was quite poorly maintained, which limits the scope of conclusions that can be drawn from this method. However, multiple soaring flights of up to 60 seconds were achieved with this method.

Finally control strategy was tested with the aim of soaring above the same ground spot while allowing for altitude variation. This strategy proved to be the most effective, with the longest test flight soaring for over 3 minutes. However, it was also the most challenging control strategy to manually fly. The main difficulty with this strategy is that the longitudinal movement of the UAV cannot be directly controlled with pitch commands. When the UAV drifts upwind of the desired ground spot, the appropriate control input is to pitch upwards, which causes the UAV to quickly gain altitude and lose airspeed. The second-order effect of this maneuver is that the UAV drifts back above its original ground spot downwind, due to its reduced airspeed. Conversely, when the UAV drifts downwind from the intended soaring spot, the correcting control input is to pitch forward, causing the UAV to dive downwards with the second-order effect of gaining airspeed and reaching its intended soaring location further upwind.

However, in practice, it was not possible to maintain position directly above the intended ground spot. When attempting to maintain a position directly above the intended ground spot, the pilot encountered difficulty due to the second-order control of the longitudinal position. As a result, the UAV's flight path exhibited a slight oscillation when viewed from the perspective of the wind vector moving from left to right. This oscillation was characterized by a clockwise motion, where the UAV would drift downwind from the intended soaring spot, then pitch forward to dive downwards and gain airspeed to reach its intended location further upwind. This maneuver would cause the UAV to overshoot its original ground spot upwind, then pitch upwards to quickly gain altitude and bleed off airspeed. The resulting loss of airspeed would cause the UAV to drift back above its original ground spot downwind. This oscillating motion added to the dynamic nature of manual flying and required the pilot to continually adjust their control inputs to maintain roughly above designed ground spot.

7

Test Setup Discussion

7.1. Test Location and Setup

The TU Delft Open Jet Facility (OJF) is a large wind tunnel with a cross section of $2.85[m]$ x $2.85[m]$, capable of achieving wind speeds exceeding $30[m/s]$. Its large cross section makes it suitable for testing both MAVs and mid-sized UAVs in the test section. The wind tunnel produces a horizontal airflow pattern, but an updraft can be created by deflecting the airflow with an obstacle or surface in the test section. To achieve this, we used a $2.44[m]$ x $2.44[m]$ wooden board with an adjustable support to change the slope angle. We measured the slope angle using a digital level meter each time we made changes. During the test, we used Optitrack [29] to feed and log positioning data with the flight controller. We employed a safety tether to prevent the UAV from crashing into the sloped wooden board or flying inside the contraction section of the wind tunnel. During soaring flight, the tether was kept slack to allow free movement of the UAV. An image of the test setup is shown in Figure 7.1.

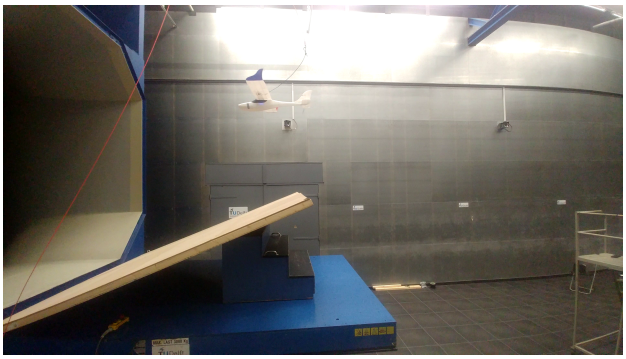

Figure 7.1: Experimental test setup in Open Jet Facility.

The properties of the UAV are listed in Table 7.1, and an image of the model is displayed in Figure 7.2. During soaring flight, the landing gear is removed to reduce drag. Additionally, in preparation for the OJF tests, the propeller was removed, and a small ballast was added to the nose of the aircraft. During the outdoor test used to determine the glide polar, a folding propeller was attached to the UAV to reduce additional drag and windmilling during soaring flight.

Table 7.1: Eclipson Model C Properties - Indoor test

Wingspan	$1100\ mm$
Length	$760\ mm$
Mass	$660\ g$
Wing Surface	$18\ dm^2$
Wing Loading	$37\ g/dm^2$
Stall Speed	$7.5\ m/s$
Maximum Speed	$18\ m/s$
Nominal Endurance	$45\ min$

Figure 7.2: Experimental test setup in Open Jet Facility.

7.2. Windfield Simulation

While it is not strictly necessary to know the wind field a priori for the controller implementation, understanding it is essential for analyzing and visualizing the test results. To this end, we used Ansys to perform computational fluid dynamics (CFD) simulations [30]. Although we only required the wind field along the vertical center plane of the test section, we opted for a 3D CFD simulation to achieve greater accuracy. The simulation was conducted based on the geometry illustrated in Figure 7.3.

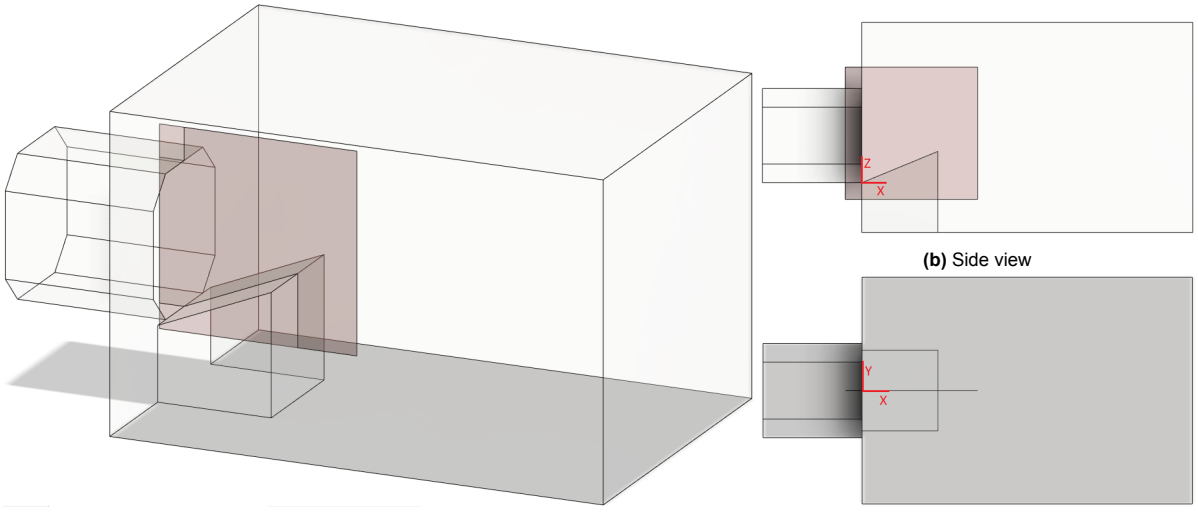

(a) 3D view **(b)** Side view **(c)** Top view

Figure 7.3: CFD geometry Open Jet Facility and horizontal slice test section.

The center plane of the test section in the wind tunnel is the key area of interest. We defined a $4[m]$ x $4[m]$ square on the horizontal center XZ plane, spanning $[-0.5X, 3.5X]$ and $[-0.5Z, 3.5Z]$, with the origin at the base of the slope. In this slice, we used a rectangular mesh with a spacing of $0.04[m]$.

We determined the wind velocity component at each node through tetrahedral interpolation of the wind velocity components in the CFD simulation. Figure 7.4 shows the resulting velocity components for a wind tunnel velocity of $8.5[m/s]$ and a slope of $23.2[deg]$. The horizontal wind speed component is indicated by the color scale, while the vertical wind speed component is shown with contours. Streamlines were also generated to further visualize the results.

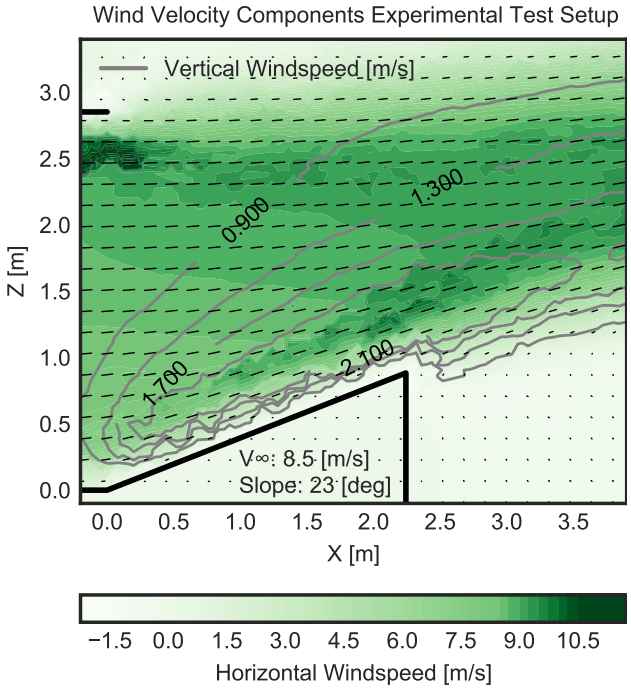

Figure 7.4: Wind velocity components in the center plane of the test section.

Due to the broad range of wind velocities and slope angles covered in the flight tests, it was impractical to conduct simulations for every possible combination. Instead, we performed CFD simulations for a discrete set of wind velocities and slopes, as detailed in Table 7.2. To obtain wind field slices for other wind velocities and slopes, we interpolated the wind velocity components between the known slices. The resulting wind field slice was then used to visualise the results for those tests.

Table 7.2: Performed CFD Simulations

		Wind velocity $[m/s]$						
		8.5	8.8	9.0	9.3	9.5	9.8	10.0
Slope Angle $[deg]$	21.3	X						
	22.1	X						
	22.6	X						
	22.7	X						
	23.2	X	X	X	X	X	X	X
	23.7	X						
	23.9	X						
	24.5	X						
	25.2	X						

7.3. Test Data

Determining the relationship between airspeed and sink rate is essential in understanding and analysing the data from the test setup. This relationship is defined by the glide polar, which we experimentally determined in an outdoor test. To perform the test, we manually flew the aircraft up to altitude using its propeller, and then manually initiated a stable gliding descent with the propeller stowed. By flying the aircraft in attitude mode, the pilot was able to maintain level flight at a constant pitch angle, allowing

us to record steady flight segments. For each segment, we logged the average horizontal speed and average sink rate as a data point for the glide polar graph. We repeated this process multiple times at different pitch angles and then determined the glide polar using third-order polynomial regression of the data points. The resulting graph is shown in Figure 7.5. To ensure consistency in the flight data, all gliding descent segments were performed at the same heading, perpendicular to the prevailing wind direction in the area on a relatively still day.

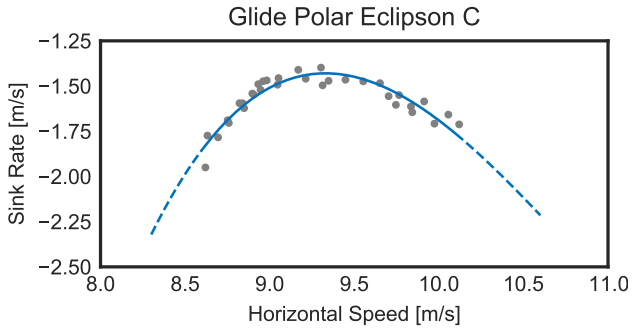

Figure 7.5: Experimental determination glide polar Eclipson Model C.

IV

Synthesis and Future Outlook

8

Conclusion

The objective of this research was to demonstrate the feasibility of autonomous orographic soaring for fixed-wing UAVs. We identified the feasible soaring region, which can be represented by a single line known as the zero excess updraft contour (ZEUC). As the longitudinal motion of a soaring UAV is an under-actuated system, we introduced the concept of a target gradient line (TGL) to provide a single degree of control freedom. We then presented an autonomous controller that enables position keeping at the intersection of the TGL and ZEUC. We validated the controller in an experimental test setup, and the results showed that it effectively maintained position on the chosen TGL without using any thrust as the UAV had no propeller. Furthermore, the position of the logged flight segments closely aligned with the expected ZEUC, which was derived from the estimated wind field and glide polar. We demonstrated that adjusting the TGL is an effective way to realize a single degree of control freedom in the system. Finally, we showed that the controller is robust to changes in the wind field, such as alterations in slope or changes in the free-stream velocity of the wind tunnel.

9

Recommendations for future work

9.1. Future Research Directions

The tests conducted in this research have provided valuable insights into the behavior of the UAV during pure orographic soaring. However, their scope was limited by the cross-section of the wind tunnel, which restricted the range of wind conditions that could be tested. Although the wind tunnel allowed for controlled testing with a known wind field, it did not offer the same range of wind conditions and variability as an outdoor environment. Therefore, additional testing is recommended to be conducted in an outdoor environment to enable a larger orographic wind field and more diverse wind conditions.

During the performed tests, the UAV was operating near the top of its glide slope, which made changes in the wind tunnel velocity have a nearly directly proportional effect on the sink rate of the UAV. This meant that no change in the soaring position could be observed when the wind tunnel velocity was adjusted. To address this limitation, testing in an outdoor environment would enable a broader range of wind velocities to be tested, thus allowing a wider envelope of the UAV's glide polar to be explored. It is important to note that when soaring in a broad airspeed range, changes in elevator effectiveness can occur, which can affect the UAV's response to controller outputs. Therefore, it is recommended to adjust the controller to handle these changes and vary the controller gains accordingly.

Finally, setting a favorable TGL can be challenging, especially without prior knowledge of the wind field. Therefore, further research is suggested on obtaining an initial soaring position to optimize the TGL for a given wind field. In addition, an analysis can be conducted to determine the range of initial starting positions that would converge to the TGL compared to starting positions that would diverge and not obtain stable soaring flight. These recommendations will broaden the scope of this research and refine the recommendations for practical implementation.

9.2. Alternative Approaches

9.2.1. Drag increasing devices

The research in this work focuses on pure orographic soaring, on the assumption that no throttle will be used during flight. As a result, the longitudinal motion of the UAV is under-constrained. This work introduces a novel controller to address this lack in control freedom. However, it should be noted that next to allowing throttle usage, there are other ways to increase the effective actuators in the longitudinal motion. One such method involves drag increasing devices such as flaps, spoilers and speed-brakes. Unlike a propulsive method, these actuators can effect the longitudinal motion of the aircraft at a much lower and discontinuous mechanical energy cost. It is conceived that when an aircraft is operating in a region with an excess in updraft, that a more traditional form of position control can be achieved with drag increasing devices. The aircraft would nominally be operated with the drag increasing devices partly enabled. Reducing drag would then have the equivalent effect of increasing throttle, while increasing drag has the equivalent effect of decreasing throttle.

With a known wind field, the feasible soaring region can be calculated. Firstly the glide polar of the UAV in clean configuration should be determined as well as the glide polar of the UAV with all drag increasing devices extended. From the wind field and two glide polars, two distinct zero excess updraft contours can be determined. It is theorised that full position control is possible in the enclosed region of both zero excess updraft contours.

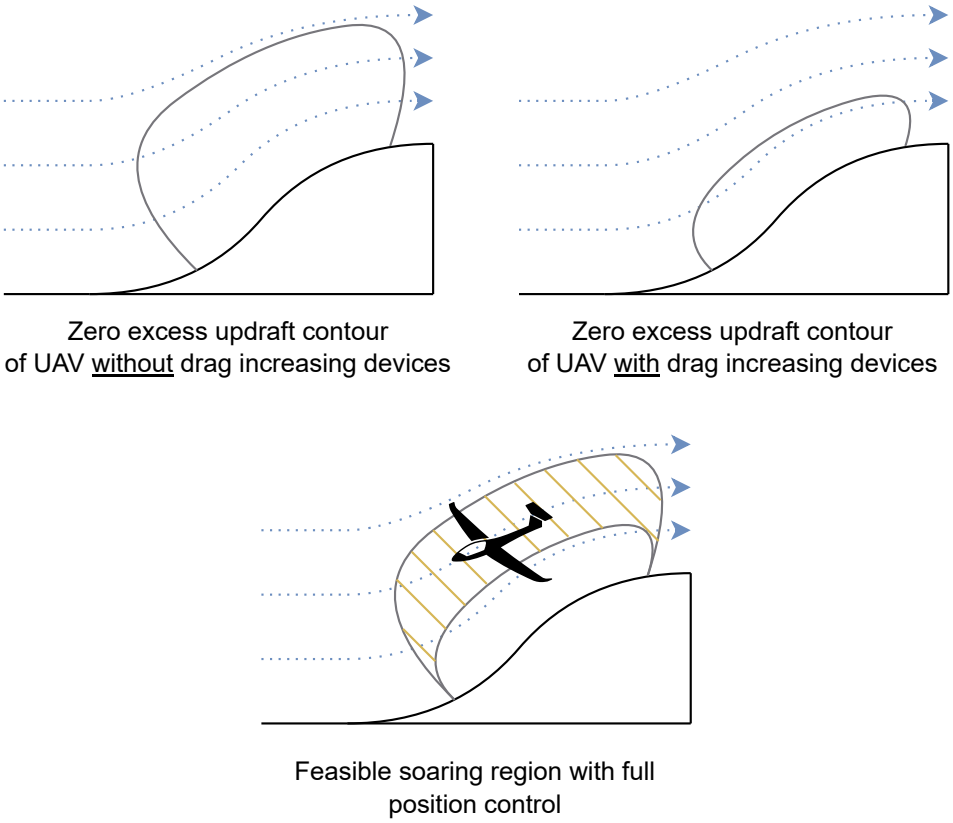

Figure 9.1: Feasible soaring region with drag increasing devices

It should be noted that this method would effectively decrease the excess updraft region of the UAV, since part of the extracted energy while soaring will always be consciously wasted as a result of the additional drag. On the flip side of this, energy harvesting approaches are deemed interesting. A small turbine could act as a variable drag inducing device. In this case, the excess updraft that this approach requires could be harvested and stored on-board to run other sub systems of the UAV.

9.2.2. Upwind zig-zag pattern

Another technique that can be considered is flying a continuous serpentine or zig-zag pattern upwind. In this case is it possible to maintain soaring flight in a region of excess updraft along a long slope or ridge. The excess energy in this region is used to maintain the kinetic zig-zagging motion. It is advantageous to explore soaring techniques where the UAV can maintain excess kinetic energy. With clever control algorithms, the additional kinetic energy can be used to more promptly adapt to changes in the wind field. Furthermore, short periods of lower updraft can be overcome by bleeding of excess kinetic energy. Note the contrast with dynamic soaring. No gradient in wind velocity is needed for above technique to work. Instead, energy is extracted from the vertical component of the deflected wind vector.

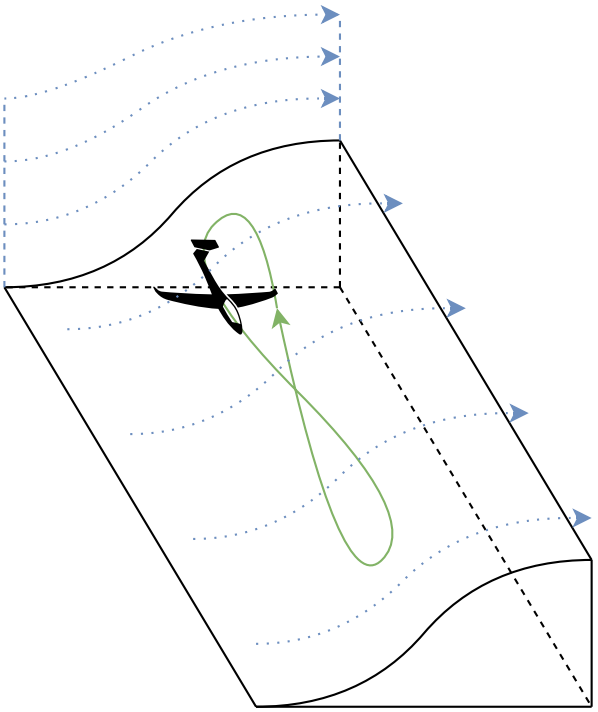

Figure 9.2: Upwind zig-zag pattern during orographic soaring.

References

[1] Drone Industry Insights. “The Drone Industry Barometer 2020”. In: (2020), p. 18. URL: www.droneii.com.

[2] Jack W. Langelaan. “Long distance/duration trajectory optimization for small UAVs”. In: *Collection of Technical Papers - AIAA Guidance, Navigation, and Control Conference 2007*. Vol. 4. 2007. DOI: 10.2514/6.2007-6737.

[3] Clarence D. Cone. “Thermal Soaring by Migrating Starlings”. In: *The Auk* 85.1 (1968). ISSN: 00048038. DOI: 10.2307/4083619.

[4] Helmut Reichmann. *Cross Country Soaring*. 1978.

[5] Michael J. Allen. “Autonomous soaring for improved endurance of a small uninhabited air vehicle”. In: *43rd AIAA Aerospace Sciences Meeting and Exhibit - Meeting Papers*. 2005. DOI: 10.2514/6.2005-1025.

[6] Caroline Dunn, John Valasek, and Kenton Kirkpatrick. “Unmanned air system search and localization guidance using reinforcement learning”. In: *AIAA Infotech at Aerospace Conference and Exhibit 2012*. 2012. DOI: 10.2514/6.2012-2589.

[7] Tim Woodbury, Caroline Dunn, and John Valasek. “Autonomous soaring using reinforcement learning for trajectory generation”. In: *52nd AIAA Aerospace Sciences Meeting - AIAA Science and Technology Forum and Exposition, SciTech 2014*. 2014. DOI: 10.2514/6.2014-0990.

[8] Javad Khaghani et al. “Analytical Model of Thermal Soaring: Towards Energy Efficient Path Planning for Flying Robots”. In: *IEEE International Conference on Intelligent Robots and Systems*. 2018. DOI: 10.1109/IROS.2018.8593907.

[9] Zsuzsa Ákosl et al. “Thermal soaring flight of birds and unmanned aerial vehicles”. In: *Bioinspiration and Biomimetics* 5.4 (2010). ISSN: 17483182. DOI: 10.1088/1748-3182/5/4/045003.

[10] Alex Fisher et al. “Emulating avian orographic soaring with a small autonomous glider”. In: *Bioinspiration and Biomimetics* 11.1 (2015). ISSN: 17483190. DOI: 10.1088/1748-3190/11/1/016002.

[11] C. White et al. “A feasibility study of micro air vehicles soaring tall buildings”. In: *Journal of Wind Engineering and Industrial Aerodynamics* 103 (2012). ISSN: 01676105. DOI: 10.1016/j.jweia.2012.02.012.

[12] Caleb White et al. “The soaring potential of a micro air vehicle in an urban environment”. In: *International Journal of Micro Air Vehicles* 4.1 (2012). ISSN: 17568293. DOI: 10.1260/1756-8293.4.1.1.

[13] A. Mohamed et al. “Scale-resolving simulation to predict the updraught regions over buildings for MAV orographic lift soaring”. In: *Journal of Wind Engineering and Industrial Aerodynamics* 140 (May 2015), pp. 34–48. ISSN: 01676105. DOI: 10.1016/j.jweia.2015.01.016.

[14] Chris P.L. de Jong et al. “Never landing drone: Autonomous soaring of a unmanned aerial vehicle in front of a moving obstacle”. In: *International Journal of Micro Air Vehicles* 13 (2021). ISSN: 17568307. DOI: 10.1177/17568293211060500.

[15] Philip L. Richardson. “Upwind dynamic soaring of albatrosses and UAVs”. In: *Progress in Oceanography* 130 (2015). ISSN: 00796611. DOI: 10.1016/j.pocean.2014.11.002.

[16] Rayleigh. “The soaring of birds”. In: *Nature* 27.701 (1883), pp. 534–535. ISSN: 00280836. DOI: 10.1038/027534a0.

[17] Joachim L. Grenestedt and John R. Spletzer. “Towards perpetual flight of a gliding unmanned aerial vehicle in the jet stream”. In: *Proceedings of the IEEE Conference on Decision and Control*. 2010. DOI: 10.1109/CDC.2010.5717109.

[18] Xian Zhong Gao et al. “Analysis and design of guidance-strategy for dynamic soaring with UAVs”. In: *Control Engineering Practice* 32 (2014). ISSN: 09670661. DOI: 10.1016/j.conengprac.2013.06.003.

[19] “Computational methods for fluid dynamics”. In: *Computers & Mathematics with Applications* 46.2-3 (2003). ISSN: 08981221. DOI: 10.1016/s0898-1221(03)90046-0.

[20] Jack W. Langelaan, Nicholas Alley, and James Neidhoefer. “Wind field estimation for small unmanned aerial vehicles”. In: *Journal of Guidance, Control, and Dynamics* 34.4 (2011). ISSN: 15333884. DOI: 10.2514/1.52532.

[21] J.D. Anderson. *Fundamentals of Aerodynamics*. 6th international ed. New York, United States: McGraw Hill Education, 2017.

[22] D. J. Acheson. “Elementary Fluid Dynamics”. In: *The Journal of the Acoustical Society of America* 89.6 (1991). ISSN: 0001-4966. DOI: 10.1121/1.400751.

[23] A. LAMBREGTS. “Vertical flight path and speed control autopilot design using total energy principles”. In: 1983. DOI: 10.2514/6.1983-2239.

[24] PX4. “PX4 Autopilot User Guide”. In: (2021). URL: https://docs.px4.io/master/en/flight_stack/controller_diagrams.html.

[25] Paparazzi Autopilot. “Paparazzi Control Loops”. In: (2021). URL: https://wiki.paparazziuav.org/wiki/Control_Loops.

[26] JCGM. *International vocabulary of metrology*. 2008. URL: https://www.bipm.org/utils/common/documents/jcgm/JCGM_200_2008.pdf.

[27] Mai A. Al-Ammar et al. “Comparative survey of indoor positioning technologies, techniques, and algorithms”. In: *Proceedings - 2014 International Conference on Cyberworlds, CW 2014*. 2014. DOI: 10.1109/CW.2014.41.

[28] iNav. *iNavFlight*. URL: https://github.com/iNavFlight.

[29] Optitrack. *Motion Capture Systems*. URL: http://www.optitrack.com/.

[30] ANSYS. *Ansys® Academic Research Fluent, Release 19.5.0*. 2019.